Alpine ductile deformation of the upper Iberian collided margin (Eaux-Chaudes massif, west-central Pyrenean hinterland, France)

Norbert Caldera[1], Antonio Teixell[1], Albert Griera[1], Pierre Labaume[2] and Marc Guardia[1]

[1]Departament de Geologia, Universitat Autònoma de Barcelona, 08193 Bellaterra (Barcelona), Spain

[2] Géosciences Montpellier, Université de Montpellier, CNRS, 34095 Montpellier, France

Corresponding author: Norbert Caldera (email: norbertcg4@gmail.com)

ABSTRACT

The Eaux-Chaudes massif provides keys to unravel the deep-seated deformation of the Iberian rifted margin during the Alpine orogeny in the Pyrenees. The massif conforms to an inlier of upper Cretaceous carbonate rocks within the Paleozoic basement of the western Axial Zone, originally deposited in the upper margin shelf before the Cenozoic collision. New geological mapping and cross-section construction lead to the description of the lateral structural variation from a km-scale fold nappe in the west to a ductile, imbricate fold-thrust fan in the east. The transition from a Variscan pluton to Devonian metasediments underlying the autochthonous Cretaceous induced this structural change. Recumbent folding, which involved upper Paleozoic rocks, was facilitated by a lower detachment in Silurian slates and an upper detachment in an

overlying Keuper shale and evaporite thrust sheet. Remains of this allochthonous sheet form shale and ophite bodies pinched within the upper Cretaceous carbonates, conforming unusual tertiary welds. Ductile shear in the overturned limb of the Eaux-Chaudes fold nappe imparted strong mylonitic foliation in carbonate rocks, often accompanied by N-S stretching lineation and top-to-the-south kinematic indicators. The burial of the massif by basement-involved thrust sheets and the Keuper sheet, along with their Mesozoic-Cenozoic cover, account for ductile deformation conditions and a structural style not reported hitherto for the Alpine Pyrenees. Two hypotheses for the tectonic restoration of this part of the Pyrenean hinterland are proposed in this work.

1. INTRODUCTION

How did inversion tectonics occur along collided continental margins? This is a complex question that depends on the specific geodynamic history within the Wilson Cycle (e.g. Manatschal et al., 2021). During the early stages of orogeny, tectonic inversion is mainly controlled by inherited factors such as the mechanical stratigraphy of the sedimentary cover and the nature of basement structures formed during previous tectonic events (e. g. Butler et al., 2006). At upper crust levels, contractional deformation typically occurs by the reactivation of extensional faults and by the development of detachment levels following weak mechanical horizons as salt and shale units. In foreland fold-and-thrust belts, synorogenic sediments give key information to decipher this early history, but in orogenic hinterlands, where polydeformed basement rocks dominate in outcrop, constraining the inversion tectonics of a particular event is challenged by the absence of unequivocal markers.

The Wilson cycle in the Pyrenees is well-documented and divided into two main stages. It commences with the Mesozoic rifting, which culminates at mid-Cretaceous times (Aptian to early Cenomanian) with hyper-extension of the Iberian and Eurasian rifted margins and mantle exhumation (e.g. Jammes et al., 2009; Lagabrielle et al., 2010). After a period considered as a post-rift stage, the extension cycle is followed from the late Santonian by the late Cretaceous-Cenozoic orogenic stage which can be subdivided into: (1) the initiation of the convergence involving mantle subduction, and (2) the main collision and deformation of the continental margins (Mouthereau et al., 2014; Teixell et al., 2016; Ford et al., 2022). Both compression stages are separated by a period of quiescence during the Paleocene (e.g. Ford et al., 2016, 2022; Ternois et al., 2019). The characteristic non-cylindricity of the Pyrenean orogen has been attributed to the extensional inheritance (e.g. Chevrot et al., 2018; Manatschal et al., 2021), especially accounting for the mechanical weakening of the basement. Saspiturry et al. (2022) recently postulated crustal-scale transfer zones partitioning the western part of the Pyrenees in an ensemble of narrow segments favouring the lateral structural variation.

The purpose of this paper is to extend the structural study of the km-scale ductile fold nappe documented by Caldera et al. (2021) for a section of the Eaux-Chaudes massif (ECM) of the Pyrenean hinterland (western Axial Zone), which formerly constituted the upper part of the Iberian rifted margin. The ECM preserves an upper Cretaceous inlier between units of Paleozoic metasedimentary and igneous rocks, previously deformed by the Variscan orogeny (Ternet, 1965) (Fig. 1). The Cretaceous platform carbonate rocks of the ECM constituted the shelf of the Iberian margin during

69 the late Cretaceous post-rift stage (Fig. 1c), later deformed during the Pyrenean
70 collision into a large fold nappe. The occurrence of the upper Cretaceous rocks in this
71 part of the Pyrenean hinterland provides a clue to the Cenozoic deformation, often
72 blurred by the dominant basement exposure of the Axial Zone (Fig. 1b). Ductile
73 basement-involved folding and moderate temperature (around 350ºC) reported by
74 Caldera et al. (2021) in the ECM account for deformation conditions never reported
75 hitherto for the Pyrenean orogeny.

76 Here, we show that the fold nappe reported by Caldera et al. (2021) passes
77 laterally to a ductile fold-thrust imbricate fan in the upper Cretaceous, and we enlarge
78 the study to the upper thrust sheets that buried the ECM, which favoured the observed
79 ductility (Fig. 2). We argue that the lateral structural variation in the ECM is determined
80 by lower (within the Paleozoic basement) and upper (within the Triassic of the upper
81 thrust sheets) detachment levels and by the occurrence of a strong igneous body
82 intruded in the autochthonous Paleozoic metasediments.

83

84 **2. TECTONIC FRAMEWORK**

85 Two rift stages (Permo-Triassic and late Jurassic-early Cretaceous) and two
86 orogenic episodes (Variscan and Alpine-Pyrenean) have defined the structural
87 architecture of the Pyrenees. The Variscan orogeny configured the Paleozoic basement
88 structure between ca. 380 Ma – 280 Ma (Cochelin et al., 2017, and references therein),
89 and culminated with the intrusion of granitic plutons around 300 Ma. The Permo-Triassic
90 extension is recorded by terrestrial red beds, starting in the study area with siliciclastic
91 sandstones and conglomerates of the Lower Triassic Buntsandstein facies. In the

Pyrenean domain, the Buntsandstein is overlain by red-green claystones and salt of Keuper facies (Biteau et al., 2006; Ortí et al., 2017), containing Muschelkalk marine limestone intercalations (Stevaux & Winnock, 1974). The Keuper facies host abundant subvolcanic bodies of dolerites ("ophites"). The main rifting in the Pyrenees occurred during early and mid-Cretaceous times inducing a strong crustal stretching (Lagabrielle & Bodinier, 2008; Jammes et al., 2009; Lagabrielle et al., 2010; Masini et al. 2014; Mouthereau et al., 2014; Tugend et al., 2014; Teixell et al., 2016; Grool et al., 2018; Espurt et al., 2019; Manatschal et al., 2021). As a result, the mantle was exhumed between the Iberian and Eurasian rifted margins with maximum basin subsidence in the Albian-early Cenomanian, and the pre- and syn-rift sediments where locally affected by HT-LP metamorphism (e.g. Golberg 1987; Golberg & Leyreloup, 1990; Lagabrielle et al., 2010; Clerc & Lagabrielle, 2014; Clerc et al., 2015; Ducoux et al., 2021). Today, the rift axis is represented by the Mesozoic sediments of the North Pyrenean Zone (NPZ) which was tectonically inverted as a large pop-up structure during the Pyrenean orogeny.

Within the Cretaceous rift, a transition from syn- to post-rift sedimentation is ascribed to the mid-Cenomanian, recorded by a regional-scale unconformity (e.g. Debroas, 1987, 1990) on which expansive late Cenomanian deposits overlap the basement and lower Triassic rocks of the rift shoulders. During the Late Cretaceous, shallow platform carbonates ("Calcaires des Cañons"; Fournier, 1905) were widely developed in both the Iberian and the European upper margins, while the former rift axis still accumulated turbidite deposits (e.g. Cuvillier et al., 1964; Puigdefàbregas & Souquet, 1986; Floquet et al., 1988; Razin, 1989). Today these shelf carbonates

115 constitute the bulk of the Eaux-Chaudes massif, where they overlie Devonian
116 metasediments and the late Carboniferous Eaux-Chaudes pluton (Debon, 1976, 1996;
117 Ternet et al., 2004; Izquierdo-Llavall et al., 2012).

118 The Pyrenean orogeny took place from the late Santonian (ca. 84 Ma) to the
119 early Miocene (ca. 20 Ma). It caused: 1) the subduction of the exhumed mantle tract
120 and the overlying rift-axis inversion, including the shortening of previous salt diapirs, and
121 the flexure-driven drowning of the post-rift platforms giving rise to flysch deposition, and
122 2) the collision of the margins, which led to the subduction of the Iberian lower crust and
123 the development of a south-verging, basement-involved thrust stack in the Iberian upper
124 crust. (Teixell et al., 2016, 2018). The ECM and overlying thrust sheets, now in the
125 Pyrenean hinterland of the northern Axial Zone, uniquely record the compressional
126 deformation of the Iberian margin, from the shelf to the hyperextended zones.

127

128 **3. STRUCTURAL AND STRATIGRAPHIC DOMAINS IN THE STUDY AREA**

129 The stratigraphic record of the ECM is well-constrained (e.g. Ternet et al., 2004)
130 and is clue in the recognition of the structural setting. Below, we first expose the
131 stratigraphy (section 3.1.), and then the tectonic configuration of the study area (section
132 3.2.), which consists of four main tectono-sedimentary domains (Fig. 3) arranged from
133 bottom to top as: 1) The Gavarnie nappe with upper Cretaceous carbonate rocks
134 unconformable on Paleozoic metasediments and granite, with scarce Buntsandstein
135 remnants in between (Fig. 2), 2) the Eaux-Chaudes nappe (cf. Fig. 3 and text below),
136 with allochthonous upper Cretaceous carbonates and Paleozoic metasediments
137 involved in complex folding. 3) the Paleozoic-bearing thrust sheets overlying the ECM,

138 comprising metasedimentary basement rocks with local Buntsandstein pods and
139 Keuper, and finally 4) the assemblage of allochthonous Keuper facies of the Bedous
140 unit, overlying all the units described above (Fig. 1c), and the Chaînons Béarnais Belt of
141 the North Pyrenean Zone consisting of a Jurassic and Lower Cretaceous succession
142 detached on the Triassic Keuper. This last succession is affected by low-grade thermal
143 metamorphism inherited from the Cretaceous rifting.
144
145 **3.1. Stratigraphy of the Eaux-Chaudes massif and surroundings**
146 ***3.1.1. Paleozoic basement and lower Triassic***
147 The pre-Mesozoic basement around the ECM consists of upper Paleozoic low-
148 grade metasedimentary rocks (Fig. 4). The oldest unit in the area corresponds to
149 Silurian black slates (Mirouse, 1962), with interbedded thin black limestone layers. It is
150 considered as the main regional detachment level for the Paleozoic of the Axial Zone
151 (e.g. García-Sansegundo et al., 2011, and references therein). Above this unit, an
152 approximately 400 to 500 m thick succession of interlayered pelites, limestones,
153 sandstones and quartzites of Devonian age is observed, followed by a few hundred
154 meters thick succession of clastic turbidites and limestones of Carboniferous age (Culm
155 facies; Delvolvé, 1987). These rocks host the Eaux-Chaudes granitic pluton, which is
156 late Carboniferous in age (301 +/- 9, Guerrot, 2001) (Fig. 2). In some thrust sheets
157 overlying the ECM, an azoic succession of limestones and schists, with local sandstone
158 layers, is tentatively attributed to the Carboniferous (Ternet et al., 2004; Labelled hCM
159 in Fig. 4).

160 Discontinuous lower Triassic conglomeratic and sandy deposits (Buntsandstein
161 facies) rest unconformably over the Paleozoic basement. In the ECM and overlying
162 thrust units, pre-Cretaceous erosion removed a vast volume of Buntsandstein, but some
163 pods have been preserved. They form useful markers to constrain boundaries of
164 stratigraphic nature and polarity relationships between the upper Cretaceous and
165 Devonian limestones of the ECM.
166
167 ***3.1.2. Allochthonous Triassic sheet***
168 The middle-upper Triassic Keuper (Fig. 4) consists of a melange of claystones,
169 cargneules, Muschelkalk limestones, and ophites (Ternet, 1965; Ternet et al., 2004).
170 Salt is not observed at the surface but is well documented nearby in the subsurface in
171 adjacent basins of the northern Pyrenees (e.g. Biteau et al., 2006; Ortí et al., 2017; Soto
172 et al., 2017). The Keuper is not found along the main unconformity between the
173 Paleozoic basement and the upper Cretaceous carbonates of the ECM but forms an
174 allochthonous sheet (the Bedous unit) emplaced over the upper Cretaceous (Caldera et
175 al., 2021; Figs. 2, 3).
176
177 ***3.1.3. Upper Cretaceous***
178 The Cretaceous stratigraphy of the ECM has been thoroughly investigated in
179 prior works (e.g. Casteras, 1956; Casteras & Souquet, 1964; Ternet, 1965; Alhamawi,
180 1992). It is characterized, from bottom to top by a carbonate platform succession (from
181 Cenomanian to Santonian) followed by shale and flysch deposits (Campanian-
182 Maastrichtian) (Fig. 4).

183 At the base of the upper Cretaceous stratigraphic succession, the Cenomanian
184 with a maximum thickness of ca. 25 m, unconformably lies on the Paleozoic basement
185 or the Buntsandstein. Occasionally, it begins with a quartz-rich microconglomerate or
186 coarse-grained sandstone, followed by a succession of grainstones to mudstones and
187 wackestones with *Praealveolina* and *Pseudocyclammina*. The transition to the Turonian
188 is highlighted by packstone to mudstone deposits featuring a *Chrysalidina* and
189 *Nezzazata* fossil content. Debris of echinoderms, *Pithonella, Halimeda ellioti* and
190 *Globotrunca helvetica bolli* are also characteristic of this unit (Conard & Rioult, 1977).
191 The Turonian limestone shows in general a varying thickness, with a maximum of 80 m
192 (Alhamawi, 1992). This variation hampers the recognition of the transition to the
193 Coniacian which corresponds to partially dolomitized grainstones and packstones with a
194 maximum thickness of ca. 40 m (Ternet et al., 2004), and dominated at the base by
195 debris of *Hippurites* rudists, polypers, gasteropods and foraminifera. To the top of the
196 sequence, there is a succession of packstones to wackestones with benthic
197 foraminifera, rudists, oysters, and polypers. In the southern flank of the Arcizettes
198 Mountains (Fig. 2), a ~40 m thick layer of dark dolomitized limestones is observed
199 constituting a reference horizon recognizable laterally along 2 km.
200 The Santonian is a massive white limestone unit, with a thickness of ca. 250 m
201 (Ternet, 1965), forming the tallest reliefs of the ECM. It begins with microconglomerate
202 or very coarse sandstone cemented by calcite and containing rounded quartz grains.
203 The white limestone contains decimetric levels of slightly sandy packstones with high
204 content of *Lacazina* and bivalve debris. The end of the Santonian is characterized by a
205 6 to 30 m layer of limestone with chert nodules, a characteristic key level in the western

206 Axial Zone (Souquet, 1967; Teixell et al., 2000) (Fig. 2), easy to recognize in the field.
207 Locally, the Santonian limestone is followed by 10 to 15 m of calcareous shales with a
208 wide variety of microfauna and fossils such as echinoids, benthic and pelagic
209 foraminifera. The top of the upper Cretaceous sedimentary record of the ECM is
210 composed of an alternation of pelites and sandstones up to several hundred meters
211 thick referred to as the Campanian flysch. Sandstones show grain-size gradation and
212 cross-stratification with quartz grains and white-mica slats, with mainly benthic
213 microfauna in the sandstones (e.g. *Orbitoides media, O. tissoti, Nummofallotia*
214 *cretacea*), and pelagic microfauna in the pelites (e.g. *Globotruncata elevata, G. rosetta*)
215 (Ternet et al., 2004).

216 The upper Cretaceous limestones represent the post-rift shelf in the upper
217 Iberian margin. Relatively stable episodes of regression and transgression determined
218 its facies deposition over time. The transition from the platform limestones to the shales
219 and flysch-type sediments of the uppermost Cretaceous mark an abrupt deepening of
220 the margin attributed to foreland flexure in the early steps of the Pyrenean orogeny
221 (Teixell, 1996; Labaume et al., 2016).

222

223 **3.2. Structural units**

224 ***3.2.1. The Gavarnie and Eaux-Chaudes nappes***

225 The Eaux-Chaudes nappe (ECN) comprises the Eaux-Chaudes fold nappe
226 (ECFN) and corresponds to the first allochthon unit with respect to the Gavarnie nappe
227 (Fig. 3). The ECFN is observed on both sides of the Ossau Valley (Fig. 5) and
228 described by Caldera et al. (2021). This fold involves the upper Cretaceous carbonates

and the upper Paleozoic succession that occupies the fold core. The recumbent limb directly rests above the relative autochthonous upper Cretaceous carbonates of the Gavarnie nappe, preserving decametric pinched bodies of Keuper facies in between (Sup. 1). Large-scale recumbent folds have not been previously reported in the context of the Alpine Pyrenees but are documented in the Paleozoic basement where they are attributed to the Variscan orogeny (Aerden & Malavieille, 1999; Matte, 2002, and references therein; Bastida et al., 2014). Carbonates from the overturned limb attest for strong ductile deformation while the normal limb and the autochthon are lowly-deformed, preserving sedimentary textures and fossil content, and featuring a spaced pressure-solution cleavage (Caldera et al., 2021). The autochthonous upper Cretaceous carbonates continue to the west as a simple north-dipping monocline and limit the western termination of the Axial Zone (Fig. 1a, b).

To the east, in the Valentin valley, the upper Cretaceous of the ECN has been eroded and the unit comprises only Devonian sediments in the hanging-wall of the Eaux-Bonnes thrust (Bresson, 1903). In this area, it overrides the upper Cretaceous carbonates of the Gavarnie nappe affected by ductile deformation in the Pic de Ger fold-thrust fan (Figs. 2, 3, 5). The transition between the lowly-deformed autochthon, in the west, to the fold-thrust fan, in the east, occurs through a relatively narrow transfer zone, here named the Gourzy transfer zone, and located between the Pic du Gourzy and Montcouges, and passing by Les Eaux-Bonnes village to the north (Figs. 2, 3, 5). This transfer zone consists of a high-angle west-dipping tear fault system, which causes a recess of the ECN, passing from the far-reaching recumbent fold nappe to the west to the Devonian in the hanging wall of the Eaux-Bonnes thrust to the east. The Pic de Ger

252 ductile fold-thrust system is interpreted to partly take over the shortening of the ECFN to
253 the east (see below).
254
255 ***3.2.2. The Paleozoic nappes above the Eaux-Chaudes fold nappe***
256 The ECFN is overlain by a stack of basement-involved thrust sheets (Fig. 3), first
257 reported by Majesté-Menjoulas (1968) and later mapped by Ternet et al. (2004). We
258 define three units that are described below from bottom to top in the pile, using a
259 description which partly differs from the previous reports. The first unit overlying the
260 ECFN is the Montagnon d'Iseye fold nappe (MIN), located on the western edge of the
261 massif (Labaume & Teixell, 2020; Caldera et al., 2021). The structure of the MIN
262 corresponds in the southern part to a south-verging recumbent fold with a ~2 km-long
263 overturned limb outlined by the Triassic Buntsandstein and cored by Carboniferous
264 rocks, while in the northern part it comprises Devonian and Carboniferous strata. Late
265 normal faults cut both the MIN and the Cretaceous and Paleozoic core of the underlying
266 ECFN (Fig. 2). The second unit corresponds to the Montagne Verte nappe (MVN) (Fig.
267 3), formed by upper Devonian to Lower Carboniferous metasediments. From west to
268 east, this unit widens cartographically up to ~3.5 km wide in the eastern limit of the
269 study area (Fig. 3). No overturned limb was identified in this unit. The uppermost
270 basement-involved unit is the Cinq-Monts nappe (5MN) (Fig. 3), which also contains an
271 overturned limb at its front, defined by the Buntsandstein beds. In particular, the 5MN
272 features a thrust fault mapped by Ternet et al. (2004) and sealed by the Buntsandstein
273 which can be thus attributed to the Variscan orogeny (Fig. 2).
274

3.2.3. The Lakora thrust system and the Chaînons Béarnais Belt

The Eaux-Chaudes massif and the Paleozoic-bearing thrust sheets are overlain by the Lakora thrust system (red and blue lines in Fig. 3). The Lakora thrust system is related to the inversion of the Iberian rifted margin from the latest Cretaceous (Teixell, 1993, Teixell et al., 2016). The main Lakora thrust *s.s.* (as proposed by Teixell, 1993) in the study area carries the Jurassic-Lower Cretaceous sedimentary rocks of the Chaînons Béarnais Belt (CBB) from the North Pyrenean Zone (NPZ) to the south (red line in Fig. 3). At its base, it is possible to observe a thick Keuper horse (the Bedous Triassic unit of Labaume & Teixell, 2020) (Fig. 3), whose sole thrust is here referred to as the Lower Lakora thrust (LwLT; blue lines in Fig. 3). The CBB is a salt-detached fold-and-thrust system made of middle Triassic to lower Cretaceous rocks from the former rift axis, affected by diapiric structures and containing mantle (lherzolite) lenses (Labaume & Teixell, 2020). Two outliers of the CBB are preserved above the western termination of the Montagnon d'Iseye nappe (MIN): the Tacha and Bergon klippes **(**Figs. 2, 3a). Scarce remnants of siliciclastic conglomerates attributed to the Albian Mendibelza formation (Ternet, 1965), characteristic of the Lakora thrust sheet to the west of the Axial Zone, have been preserved over the Triassic Keuper or directly on the footwall upper Cretaceous (Figs. 2, 3, 5). In the study area, the characteristic shortcut of the Paleozoic underlying the Mendibelza conglomerate in the Iguntze massif to the west (Teixell, 1993), and shown in Figure 3b, is lacking.

4. STRUCTURAL SECTIONS OF THE EAUX-CHAUDES MASSIF

297 To describe the structure of the ECM and its lateral variation, we present six new
298 cross-sections (Figs. 6, 8) and several interpreted outcrop images or panoramas (Figs.
299 7, 9). The sections are oriented approximately N-S, perpendicular to the dominant
300 structural trend, and have been constructed from original fieldwork and complemented
301 by additional data from previous published maps and cross-sections (e.g. Ternet, 1965,
302 Ternet et al., 2004, Labaume & Teixell, 2020, Caldera et al., 2021). The Move software
303 (Petroleum Experts) was used for the managing of map data and to constrain surfaces
304 and geolocation of structural data in 3D.
305 The description of the sections is divided into two parts to account for the
306 different structural characteristics between the western and eastern sectors (Fig. 2).
307 While in the western sector (Ossau Valley), the structure of the ECM is dominated by a
308 large-scale allochthonous fold nappe, the ECFN involving the upper Cretaceous (Figs.
309 3, 6), in the eastern sector (Pic de Ger massif) the structure is characterized by an
310 imbricate fold-thrust fan in the upper Cretaceous of the Gavarnie nappe (Fig. 8).
311
312 **4.1. Western sector (Ossau Valley): the Eaux-Chaudes fold nappe**
313 The general structure of the ECM has been classically interpreted as a duplex
314 with a roof thrust carrying Paleozoic rocks over the upper Cretaceous (Ternet, 1965;
315 Déramond et al., 1985; Dumont et al., 2015; Cochelin et al., 2017). Just a short,
316 overturned fold limb was reported by Ternet (1965) in the front of the structure without
317 continuity to the north. Recently, the structure of this western sector has been
318 reinterpreted as a km-scale, south-vergent recumbent fold nappe with a large,
319 overturned limb (Caldera et al., 2021) (Fig. 6). The Eaux-Chaudes section (S2 in Fig. 6)

has been improved from the one presented in Caldera et al. (2021). In this contribution, we further document the structure by enlarging the analysed area and providing new structural data and field images (Figs. 2, 5, 7, 9). Due to a general westward plunge, constraints for the upper thrust sheets are stronger to the west, while in the eastern sections, the structures projected above topography have larger uncertainties.

The autochthonous upper Cretaceous (i.e. the Mesozoic cover of the Gavarnie nappe, Figs. 2, 5) lies unconformably on the Eaux-Chaudes granite and remains weakly deformed along this sector, preserving sedimentary textures and unstrained large fossils such as rudists or gastropods (Ternet, 1965; Caldera et al., 2021). In the ECFN, the upper Cretaceous succession is not always complete but locally preserved up to the Campanian flysch (i.e. below the Montagnon d'Iseye thrust in S1). The normal limb is weakly deformed while features observed in the upper Cretaceous carbonates of the overturned limb indicate top to the south shearing, developed under ductile conditions and moderate temperatures (315ºC to 328°C in the normal limb; 334ºC to 355°C in the overturned limb and autochthonous; Caldera et al., 2021). Examples of this ductility at large and small scales are evidenced by bedding-parallel mylonitic foliation, mineral stretching lineation, S-C composite fabrics and other asymmetric kinematic indicators (i.e. calcite crystal-shape fabrics, dolomite porphyroclasts).

The fold nappe plunges to the west following the general trend of the western Axial Zone. Although there exist some small differences in the fold shape across the three sections (Fig. 6), the overall geometry is consistent. The overturned stratigraphy is constrained by the presence of Buntsandstein pods, which show way-up criteria (crossbedding, grain-size grading) indicating a reverse polarity (Caldera et al., 2021),

343 along the contact between Paleozoic and upper Cretaceous rocks of the fold core. It is
344 worth mentioning the strong thinning of the upper Cretaceous in the overturned limb
345 eastwards from section 1 to section 3 (Fig. 6).

346 The hinge zone of the recumbent fold is box-shaped featuring ductile deformation
347 in the Cretaceous rocks evidenced by stretched fossils and grain recrystallization
348 observable in thin sections, while these rocks remained weakly deformed in the normal
349 limb. A complex network of calcite veins is also observed along the unconformity
350 between the Paleozoic and upper Cretaceous. The thrusted syncline of the ECFN is
351 linked in depth and eastwards with the Eaux-Bonnes thrust (e.g. Bresson, 1903, Ternet
352 et al., 2004), well-traced in the Valentin valley ("accident du Valentin" in Ternet, 1965)
353 (Fig. 2). Several Keuper facies and ophite bodies remain trapped in between the
354 overturned limb of the ECFN and the autochthon (Figs. 2, 5 and Sup. 1, in
355 supplementary material), which are remains of the allochthonous Keuper sheet (Bedous
356 unit) of the overlying Lakora unit pinched in the synformal zone between both limbs (i.e.
357 a tertiary weld *sensu* Jackson & Hudec, 2017) (Caldera et al., 2021). In the Paleozoic
358 core of the fold, inherited Variscan folds of the stratigraphy can be recognized (light grey
359 lines in Fig. 7a).

360 South of the recumbent fold hinge, the autochthonous upper Cretaceous features
361 small steep north-vergent back-thrusts (Caldera et al., 2021) (Figs. 6, 7), associated
362 with the tilting of the northern Axial Zone. These thrusts are visible in the western side of
363 the Ossau Valley, where they offset the Paleozoic basement and the upper Cretaceous
364 alike (section S1 in Fig. 6 and Fig. 7a; Caldera et al., 2021). The number of these north-
365 vergent structures increases from west to east, evolving from a simple back-thrust (S1)

366 to a small antiformal stack (section S3 in Fig. 6 and Fig. 7b). On the eastern side of the
367 Ossau Valley, on the southern slopes of the Pic du Cézy, they cause repetitions of the
368 upper Cretaceous and Keuper thrust sheet (Sections S2 and S3 in Fig. 6 and Fig. 7b).
369 Ophite bodies are also pinched between the hinge of the ECFN and the imbricate
370 sheets.

371 The Paleozoic stratigraphy involved in the ECFN follows the large anticlinal
372 geometry, but inherited Variscan folds determine more complex features (Fig. 6).
373 Silurian slates form the fold core but they are locally directly in contact with the
374 overturned upper Cretaceous (see S2 section), and to the north, they are pinched by
375 the Devonian limestones accommodating top-to-the-south shearing.

376 Over the ECFN in this sector, we have represented the Paleozoic upper thrust
377 sheets reported above (i.e. the Montagnon d'Iseye, Montagne Verte and Cinq Monts
378 nappes). The MIN and 5MN show overturned fold limbs defined by the Buntsandstein.
379 Frequent Keuper pods are pinched between the thrust units, derived from the overlying
380 Lakora thrust sheet. Over the Keuper, the Lakora unit carries the whole stratigraphy of
381 the CBB together with Mendibelza conglomerate inliers (e.g. Figs. 3, 6, 8), which we
382 interpret separated by the Licq fault as is observed more to the west (Labaume &
383 Teixell, 2020). Of the Paleozoic nappes, the first unit over the ECFN (i.e. the MIN)
384 keeps Keuper remains in its footwall, corresponding to the Bedous allochthonous sheet
385 previously emplaced by the Lower Lakora thrust.

386

387 **4.2. Eastern sector (Pic de Ger massif): The ductile fold-thrust system**

388 The cross-sections and field-interpreted images from the eastern sector are
389 shown in Figs. 8 and 9, respectively. In this area, constraints for the upper thrust sheets
390 are scarce, except for the klippes of Keuper and Mendibelza conglomerates carried by
391 the Lakora thrust system on top of the upper Cretaceous (cropping out south of Plateau
392 d'Anouilhas, Fig. 5 and Sup.2 for location). Although intensely folded, as reported by
393 Ternet (1965), the upper Cretaceous is broadly in a right-way-up attitude, and in
394 contrast with the western sector, a long-overturned panel is not observed.
395 The structure equivalent to the allochthonous Eaux-Chaudes fold nappe is
396 largely eroded, and the continuation of its basal thrust, the Eaux-Bonnes thrust, brings
397 the Paleozoic on top of the upper Cretaceous in the Valentin valley (Figs. 2, 8). The
398 hanging wall fold structure represented in the sections is speculative and is addressed
399 in the discussion. Paleozoic-bearing thrust sheets (MIN and MVN) are completely
400 eroded above the ECM and are not represented in these sections. The upper
401 Cretaceous of this eastern sector, which is considered as autochthonous to the ECFN,
402 is notwithstanding affected by strong ductile deformation (folding, foliation and
403 stretching lineation), in contrast with the western autochthon. Cross-sections S4 to S6
404 and field images (Figs. 8, 9) illustrate a strain gradient in the autochthonous rocks that
405 increases from west to east.
406 In section S4, from south to north, the first main structure recognized is a north-
407 vergent syncline (Fig. 8a) in the Paleozoic basement and the overlying upper
408 Cretaceous rocks of the Petite Arcizette peak (Fig. 9a; peak location labelled "Pte.
409 Acz."in Fig. 5), with intensely folded Campanian flysch rocks in its core (e.g. Dumont et
410 al., 2015). This structure, trending E-W, is rapidly damped to the east. It follows to the

north a subhorizontal or north-dipping kilometric-scale panel, cut by steeply dipping normal faults and affected by hectometre-scale south-verging folds (Fig., 8a). An asymmetric E-W trending graben in Plateau d'Anouilhas (Fig. 5, 8a and Sup. 2) preserves Keuper rocks of the Bedous unit, which are allochthonous over the upper Cretaceous. A few hundreds of meters to the west of section S4, two larger klippes are observed, one carrying the Keuper rocks and the other the Mendibelza conglomerates (Ternet, 1965) (Figs 2, 5, 8a), also interpreted to have been carried by the Lakora thrust system (Fig. 3).

Further to the east (e.g. S5, Fig. 8), folding of the upper Cretaceous becomes more intense in the Pic de Ger fold-thrust fan. Two large-scale south-verging similar folds (the tight anticline-syncline pair shown in Fig. 9b), are beautifully exposed on the western slopes of Pic de Ger, and separated by a complex north-dipping thrust fault obliterated by a penetrative schistosity. The axial planes are inclined to the north by ~30º degrees (Figs. 8b, 9b). The fold limbs are strongly stretched, the hinges are thickened, and a penetrative axial plane foliation is well-developed. South-verging internal detachments within the upper Cretaceous are locally observed. The most illustrative examples are represented in section S6 in Fig. 8 and in Figs. 9c, d. The detachment is quite evident by the triangular shape of the Cenomanian limestones which have been ductily squeezed in a thrust footwall. Asymmetric, tight disharmonic folds are recognized north of the exposed detachment (Fig. 9d), evidencing a large amount of shortening. Penetrative foliation and stretching lineation are well-developed. Dolostone levels within the dominant limestones appear stretched and boudinaged.

433 Large-scale, heterogeneous dolostone boudins are folded and imbricated (Fig. 9d) and
434 foliation wraps around these bodies, which occasionally resemble large porphyroclasts.
435 Several steeply-dipping fault surfaces cutting the upper Cretaceous and
436 Paleozoic rocks contain pinched bodies of Keuper and ophites on top of them,
437 resembling salt welds (e.g. the southern border of Pic de Ger; section S5 in Fig. 8).
438 These unusual structures, which origin is discussed below, were reported by Ternet et
439 al. (2004) and exhibit lateral continuity in W-E direction along the eastern sector of the
440 ECM (Fig. 5). An example of that is the large ophite body located south of Pic de
441 Breque (Fig. 5 for location) and the continuous welded structure passing eastwards
442 through the Montcouges-Pambassibé peaks and Pic de Ger massif (Figs. 2, 5). To the
443 east, these faults rapidly fade and are not observed in S6. On the other hand, the
444 unconformity between Paleozoic and Mesozoic rocks is locally affected by small south-
445 verging imbricate thrusts affecting the upper part of the Devonian and the Cenomanian
446 under the main detachment level (S6 in Fig. 8 and Fig. 9 d).
447
448 **5. DISCUSSION**
449 Field observations and the cross-sections of the ECM indicate a complex ductile
450 deformation of the Iberian margin during the Pyrenean collision. A marked difference in
451 tectonic style is observed between the eastern and western sectors of the massif: from
452 a large-scale recumbent fold nappe, the ECFN, in the west with high strain localized in
453 the overturned limb, the structure changes eastwards to a simple thrust, the Eaux-
454 Bonnes thrust, overlying a fold-thrust fan in the footwall with strong ductile deformation
455 accommodated in the autochthonous Cretaceous succession. Several factors may have

456 contributed to the complex structure depicted in the cross-sections: 1) the structural
457 inheritance of the Paleozoic basement due to the Variscan orogeny, 2) the geometry
458 and thermal gradient of the Iberian margin due to the mid-Cretaceous hyperextension,
459 3) the mechanical stratigraphy of both the Mesozoic and Paleozoic rocks, and 4) the
460 tectonic burial by the emplacement of the upper thrust sheets. During the inversion of
461 the rifted margin, the structural configuration of the basement and sedimentary cover
462 induced the reactivation of ancient structures and the activation of several detachment
463 levels (Silurian, Keuper and intra-Cenomanian). We focus the discussion on two major
464 key questions: 1) the factors influencing the lateral variation of the ECM structure and 2)
465 the tectonic evolution of the ECM and overlying thrust units using sequential restoration
466 of two sections (S1 and S4).
467
468 **5.1. What caused the structural contrast between the fold nappe and the fold-**
469 **thrust domain? Constraints from the recumbent fold**
470 The structural variation of the fold nappe to the fold-thrust system observed in the
471 eastern sector is quite sudden and occurs through a relatively narrow transfer zone near
472 Gourzy (Figs. 2, 5, 6). The fold nappe domain coincides with the existence of the Eaux-
473 Chaudes granite pluton under the autochthon (Fig. 3). We infer from our observations
474 that the Gourzy transfer zone accommodates a structural variation where the
475 development of the recumbent fold to the west was thus favoured by the nature of the
476 footwall basement, coupled with the existence of mechanically weak layers that induced
477 both a lower and an upper detachment, i.e. the Silurian of the fold core and the
478 allochthonous Keuper emplaced over the Upper Cretaceous.

The Paleozoic basement underlying the ECM is constituted by two clearly differentiated lithological units: the upper Paleozoic metasediments and the Carboniferous granite pluton (Figs. 2, 5, 6). While the recumbent fold largely coincides with the lateral extent of the granite, the eastern fold-and-thrust fan overlies Devonian rocks (interlayered slates and black limestones), which are mechanically weaker (Figs. 2, 5, 8). The deformation in the Eaux-Chaudes granite is of low strain, with occasional minor back-thrusts, whereas the Paleozoic rocks show strong ductile deformation expressed by crenulation and folding superpositions, with a late-phase pervasive folding with southern vergence from minor to large scale. Although the age of the different folding phases (i.e. Variscan vs. Alpine) has not been unequivocally demonstrated, we suggest that the Paleozoic rocks may have experienced superposed shortening from both orogenic cycles (e.g. Sup. 3, showing Alpine foliation crossing the unconformity between the Paleaozoic and upper Cretaceous), as also hinted by Ternet (1965).

We postulate that the granite acted as a forestop, producing a strain shadow zone to the autochthon Mesozoic cover directly overlying it and enabling the transport of the fold nappe involving Paleozoic metasediments originally north of the granite. We must point out that Bresson (1906) already invoked the role of the basement granites for the nucleation of thrust nappes in the area and Ternet (1965) suggested the importance of the granite in the overall deformation.

The ECFN is bounded by two mechanically weak units, the Silurian black slates at its bottom, and the allochthonous Keuper sheet on the top of the structure, which both acted as lower and upper detachment, respectively. The Silurian detachment allowed a relatively thin upper Paleozoic section to be entrained in the fold core by top-

to-the-south shearing as proposed in Fig. 6, which in turn enabled the recumbent folding. The Silurian slates, reported as well as the basal detachment of the Gavarnie thrust (Bresson, 1903; Séguret, 1972), have also been proposed to be an effective Alpine detachment eastward of MVN in the Chiroulet and Lesponne domes (Cochelin et al., 2021). Likewise, we interpret that the upper Paleozoic thrust sheets of the study zone (MIN, MVN, 5MN) are also detached in the Silurian slates.

The allochthonous Keuper sheet, which probably contained a large proportion of salt, was also key in causing the decoupling of the upper Cretaceous from the overlying thrust sheets. This unit was attributed to the infill of an early Triassic graben later inverted (Teixell, 1993, Labaume & Teixell, 2020), to an olistostrome (Stevaux & Zolnai, 1975; Lagabrielle et al., 2010), or to an extruded salt sheet (García-Senz et al. 2019). We postulate that it was carried by the Lakora thrust system on top of the upper Cretaceous limestones previous to the activation of the Paleozoic and Eaux-Chaudes nappes. Indeed, the Keuper on the upper Cretaceous limestones was also crucial in enabling recumbent folding of the ECNF and was expelled from the underlying faulted syncline as attested by few pinched remnants (Caldera et al., 2021; Sup. 1). Hence, the combination of two detachments (the Silurian in the upper Paleozoic and the allochthonous Keuper) with the Eaux-Chaudes granite buttress effect accounts for the intense top-to-the-south shear leading to the development of the Eaux-Chaudes recumbent fold that characterizes the western part of the massif, while a deformable Paleozoic basement and a weak horizon in the lower part of the upper Cretaceous carbonates favoured the ductile fold-thrust fan in the eastern part.

5.2. Weld structures within the upper Cretaceous

A singularity of the ECM is the existence of pieces of Triassic ophite, Keuper shale and cargneule pinched within the upper Cretaceous limestones. Two main occurrences are recognised: 1) in the tight syncline between the overturned limb of the ECFN and its relative autochthon (Sup. 1), and 2) in steep fault zones cutting the right-way up succession of the eastern upper Cretaceous limestones of the massif (Figs. 5, 6).

A first-order interpretation for the origin of these features can invoke salt tectonics, assimilating the structures that host the Triassic slivers to salt welds. It could be speculated that pre-existing diapirs sourced in Keuper salt originally located under the upper Cretaceous were squeezed during the convergence producing the salt welds. This scenario could be similar to the interpreted salt structures observed in the Jurassic and lower Cretaceous rocks of the CBB (Labaume & Teixell, 2020). However, Keuper rocks are nowhere observed under the upper Cretaceous of the ECM, which is seen always unconformable directly over Paleozoic rocks or small Buntsandstein pods. Hence, we consider that the salt welds do not derive from the squeezing of regular diapirs that originally pierced the Cretaceous succession as previously interpreted by Ternet (1965) or Dumont et al. (2015), but rather must be tertiary welds derived from the squeezing of the allochthonous Keuper sheet of the overlying Lakora unit. Caldera et al. (2021) interpreted in this way the Keuper and ophite slivers in the sheared, isoclinal synform between the fold nappe and its autochthon. During the growth and amplification of synform, there was an extreme expulsion of the Triassic sheet from the fold core, producing the weld between autochthon and overturned fold limb, and favouring the

548 accumulation of Keuper facies south of the ECFN hinge (Fig. 6). Similarly, in the steep
549 welds of the eastern part of the ECM, the Keuper and ophite bodies are observed in the
550 upper part of the upper Cretaceous limestones, associated to high-angle faults (Fig. 10)
551 and just below to the Lakora detachment. These faults, that currently may show normal
552 or reverse offsets, are interpreted as former extensional faults synchronous to, or post-
553 dating, the emplacement of the Lakora thrust sheet, as for example observed in the
554 Anouilhas graben (Fig. 5 and Sup. 2), that were subsequently shortened during the
555 deformation of the ECM. The faults often show drag folds on both walls, which can be
556 described as a-type flanking folds according to the classification by Passchier (2001),
557 consistent with early extensional slip. The origin of these extensional faults is unclear,
558 but they may be attributed to flexural load by the overlying thrust sheets to the north
559 (Lakora system and Paleozoic-bearing thrust sheets). Within this context, the ophites
560 and Keuper were down-dropped along the flanking folds associated to the normal faults.
561 Subsequent shortening led to fault steepening and tightening of the flanking folds,
562 expelling the Keuper and ophites, which were locally pinched forming the observed
563 weld-like structures (Figs. 8, 11). Again, they represent an unusual kind of tertiary salt
564 welds, where the remains of an allochthonous sheet are not in the contact between the
565 subsalt and suprasalt layers, but were entrained between tightly folded subsalt rocks.
566
567 **5.3. Sequential evolution of the upper Iberian margin: the Eaux-Chaudes fold**
568 **nappe and the eastern Eaux-Chaudes fold-thrust system**
569 Restorations of sections S1 and S4 are shown in Fig. 12 and Fig. 13. The
570 sequential evolution diagrams are started at the immediate pre-orogenic stage (Mid-

571 Santonian) of the upper Iberian margin. The reconstructions are based on our field
572 observations, structural cross-sections and data compilation from previous works on the
573 west-central Pyrenees, mainly from Teixell et al. (2016) and Labaume & Teixell (2020).
574 Dashed lines in the sketches indicate the trace of the future faults in the next step. Red
575 arrows on the right border of the pictures illustrate the compressional stage while blue
576 arrows indicate the post-orogenic exhumation.
577

578 ***5.3.1. Sequential evolution of the Eaux-Chaudes fold nappe (Fig. 12)***

579 The evolution is shown in seven steps, spanning from the mid-Santonian to the present-
580 day.

581 a) During the Mid-Santonian, the Iberian margin is interpreted as a post-rift shallow-
582 water carbonate shelf (i.e. Calcaires des Cañons), directly covering the Paleozoic
583 basement in the future ECM or the Keuper of the Bedous unit in the future Paleozoic
584 nappes MIN, MVN and 5MN. The boundaries between these units are interpreted as
585 inherited late-Variscan or Mesozoic extensional faults dipping to the north.

586 The Bedous unit was limited to the north by the shelf edge and slope rupture of the
587 Iberian platform. Northwards in the basin, the Mendibelza conglomerates onlap the
588 Paleozoic basement on the necking zone of the continental margin, limited to the north
589 by a diapiric structure which will become the Licq fault. This limit is interpreted to
590 correspond to the southern limit of the CBB, which occupy the former Cretaceous rift
591 axis (Labaume & Teixell, 2020).

592 b) The early stages of the Pyrenean orogeny were marked by the deepening of the
593 upper Cretaceous shelf and sedimentation of the Campanian-Maastrichtian flysch, the

first syn-orogenic sediments. The inversion of the basin started with the transport to the south of the salt-detached fold-and-thrust system of CBB by the thin-skinned Lakora thrust (red line) (Teixell et al., 2016, Labaume & Teixell, 2020).

c) Near synchronous with the Lakora *s.s.* thrust, there was the activation of the Lower Lakora thrust (blue line) which emplaced a horse carrying most of the Bedous evaporitic unit over the future ECM. During or immediately after this stage, the sole detachment on the Silurian of the 5MN (brown line) was active and started to override the southern segment of the Bedous basement.

d-e) Progressively, the northern Paleozoic thrust sheets (MIN, MVN and 5MN) were emplaced by a propagating basement-involved thin-skinned (Pfiffner, 2017) thrust system, in a piggy-back sequence. The nappe stacking in combination with the Iberian margin flexure (e.g. Labaume et al., 2016) and the foredeep sedimentation enhanced the burial, placing the ECM at a depth of ca. 10 km. The deepest nappe in the stack, the ECFN, was the latter to be activated. While the compression progressed, the Eaux-Chaudes granite faced opposition to deformation, which was transmitted upwards and also to the rear. This fact triggered the nucleation of the antiformal fold cored by Silurian slates and Devonian layered and foliated metasediments. The persistent shortening kept the progression of the structure to a fold nappe by the hinge migration mechanism as discussed by Guardia et al. (2020).

The temperatures reached by the burial, and possibly enhanced by an inherited high geothermal gradient (Bellahsen et al., 2019; Caldera et al., 2021), facilitated the dominant ductile deformation associated with the ECFN. Meanwhile, the progressive advance of the upper units (basement units and CBB) created a regional south-directed

617 shearing favouring the hinge migration of the anticlines which turned into recumbent
618 folds. The overturned limbs of the MIN and the 5MN, formed at relatively lower burial
619 than the ECFN, are defined by siliciclastic rocks of the Buntsandstein and display a
620 short (<1 km in 5MN) to moderate length (>2 km in MIN).
621 The stacking and folding of the Paleozoic units and the ECFN provoked the folding of
622 the Keuper sheet previously emplaced on their top. The progressive growth of the
623 overturned limbs and tightening of the synclines resulted in the Keuper expulsion and
624 weld between limbs, as proposed by Caldera et al. (2021).
625 Based on tectonic-sedimentation relationships in the Jaca foreland basin, it has been
626 proposed that the Lakora and the Eaux-Chaudes nappes remained active up to Mid-
627 Eocene times (Labaume et al., 2016), by the system propagating in a broad piggy-back
628 sequence.
629 f) The southward displacement and development of the ECFN and Paleozoic-bearing
630 units were followed, from the Late Eocene, by the emplacement of the Gavarnie nappe
631 which corresponds to a change in the deformation style by the accretion of a footwall
632 sequence of thick-skinned thrusts favouring the antiformal structure of the Axial Zone
633 (Teixell, 1996; Jolivet et al., 2007; Labaume et al., 2016; Teixell et al., 2016) (Fig. 1b).
634 This stage is inferred to correspond to the full crustal collision between the Iberian and
635 European plates which developed from the Late Eocene to Early Miocene (Teixell et al.,
636 2016). It induced the uplift and arching of the previous structures, which were tilted to
637 the north in the northern limb of the Axial Zone antiform. We interpret that in the ECM,
638 local structural features such as north-verging back-thrust systems, back-folds, and sub-
639 vertical foliation were related to the Gavarnie nappe emplacement.

g) Further uplift of the ECM and adjoining areas by the emplacement of the Guarga thrust are constrained by thermochronology during the Late Eocene-Miocene (Bosch et al. 2016). Consequently, a large amount of recycled, earlier syn-orogenic deposits and Axial Zone rocks were shed into both the Jaca (Puigdefàbregas, 1975; Labaume et al., 2016; Roigé et al., 2016) and Aquitaine foreland basins (Biteau et al., 2006) (Fig. 1a). During the post-orogenic stage in the Axial Zone, there was the development of extensional faults affecting the whole stack, from the ECFN to the CBB. These faults down-dropped the 5MN and MVN to the north to a lower structural elevation than the MIN and were probably formed in the final steps of Gavarnie-related arching (Teixell, 1996) and reactivated in Quaternary times by isostatic readjusting induced by erosion (e.g. Lacan, 2008; Lacan & Ortuño, 2012; Dumont et al., 2015).

5.3.2. Sequential evolution of the eastern Eaux-Chaudes fold-thrust fan (Fig. 13)

We highlight here the most important differences from the western sector (Fig. 12). The eastern sector is characterized by Paleozoic-bearing thrust units above the ECN where the Cretaceous has been eroded. For the purpose of simplification, the post-rift stage shows a shorter basement of the Bedous unit, only represented by the future MVN and 5MN; the Triassic is inferred from the klippe observed in the eastern ECM.

During the orogenic stages, deformation was spread in the autochthonous Mesozoic and Paleozoic rocks of the eastern ECM, due to the weaker basement because of its anisotropic behaviour and the absence of the granitic pluton. In relation to the flexure of the margin by thrust sheet loading, two scenarios could explain the current

663 structural configuration involving Keuper rocks: 1) pre-alpine inherited extensional
664 structures in the Paleozoic were reactivated or 2) extensional faults were neoformed.
665 We interpret that those extensional structures were activated in the initial stages of the
666 inversion, caused by the emplacement of the northernmost thrust sheets, and previous
667 to the climax of ductile deformation in the ECM, which favoured the development of the
668 Pic de Ger fold-thrust fan and the fault reactivation.

669 The overturned limb of the ECFN is not preserved and is interpreted as a simple
670 hanging-wall anticline above the Eaux-Bonnes thrust, with a moderately- developed
671 overturned limb in the upper Cretaceous. Indeed, at variance to the western part, the
672 autochthonous upper Cretaceous is strongly ductily deformed, indicating a larger
673 accommodation of the deformation in the footwall of the ECN.

674 The eastern north-verging syncline of the Petite Arcizette (S4 in Fig. 8)
675 represents a fault-propagation fold from the back-thrust system associated with the
676 Gavarnie thrust. Further east, the steep attitude of the basement-upper Cretaceous
677 unconformity, south of i.e. Pêne Médaa (Figs. 8, 9), corresponds to the continuation of
678 the same back-folding of the Gavarnie nappe.

679

680 **5.4. Implications on the collision of the Iberian margin during the Pyrenean**
681 **orogeny**

682 The Alpine Pyrenees are characterized by two main types of tectonic structures:
683 1) thick-skinned thrusts (e.g. Gavarnie, Guarga, Broto) detached in depth and
684 enhancing the structural relief along the belt, and 2) thin-skinned thrusts (e.g. Lakora,
685 Larra, Monte Perdido, Cotiella) with shallower detachments in the Mesozoic cover or in

686 the upper Paleozoic (basement short-cuts, e.g. Teixell 1993), sometimes being able to
687 carry sheets over long distances (e.g. Teixell et al., 2018; Espurt et al., 2019). The Axial
688 Zone of the Pyrenees is usually assumed as weakly deformed in dominant brittle or
689 brittle-ductile conditions during the Alpine orogeny. From our study of the ECM
690 Mesozoic rocks in the Pyrenean hinterland, we conclude that the recumbent fold nappe
691 resulted from “ductile” thin-skinned basement-involved tectonics (nomenclature by
692 Pfiffner, 2017), in an intense simple shear deformation regime associated with
693 detachment in the upper Paleozoic (see Figs. 6, 12). This scenario also prevails for the
694 basement units MIN, MVN and 5MN which are also detached on the Silurian,
695 occasionally featuring recumbent folds on their front. All these structures represent the
696 transition between dominant thin-skinned tectonics (i.e. Lakora thrust) to thick-skinned
697 tectonics (i.e. Gavarnie thrust), and were formed in greenschist metamorphic conditions
698 favoured by considerable burial. The hypothesis of ca. 10 km of burial and the
699 consequent thermal state are consistent and supported by the (U-Th)/he
700 thermochronology of the western Axial Zone (including the ECM) which yielded Miocene
701 cooling ages of reset zircon grains (Bosch et al., 2016). Accounting for that, the thermal
702 reset of the Paleozoic basement may have been acquired during the Pyrenean orogeny
703 by a combination of structural stacking and syntectonic sedimentation burial. Indeed,
704 recently Curry et al. (2021) proposed larger exhumation (17-19 km) for the whole Axial
705 Zone of the Pyrenees, perhaps unrealistic values with our observations and
706 paleotemperature estimates from Caldera et al (2021).

707 The tectonic style at Eaux-Chaudes has not been reported thus-far in the Alpine
708 Pyrenees, evidencing basement-involved, ductile thin-skinned folding and thrusting.

Similar ductile alpine structures may have been unperceived so-far in other parts of the Paleozoic basement of the Axial Zone. The Eaux-Chaudes deformation structures may be extended ~40 km to the east (cf. Fig. 1) conforming the northern wall of the Néouvielle shear zones dated at the early Eocene (circa 50-48 Ma) by radiochronologic methods (Wayne & McCaig, 1998; Jolivet et al. 2007). In the Néouvielle granite, Jolivet et al. (2007) obtained Oligocene to Miocene fission-track cooling ages, similar to the results of Bosch et al. (2016), supporting a deep regional burial, resetting of thermochronometers, followed by a rapid Alpine exhumation. The tilting of the Axial Zone to the west also affects the ECM, covered by the Bedous Triassic sheet and the Igountze and Mendibelza massifs westwards (cf. Fig. 1a). From a regional point of view, the reconciliation with the structure of the Basque massifs is not straightforward due to the tilting and the rapid structural variation related to the influence of transverse structures such as N-S transfer zones (e.g. Saspiturry et al., 2022), similar to what occurs at a smaller scale in the ECM with the Gourzy transfer zone.

6. CONCLUSIONS

Six new cross-sections pose the scope of the remarkable structural variability within the upper Cretaceous of the Eaux-Chaudes massif along strike. The structure passes from an allochthonous, large-scale recumbent fold core by Paleozoic sediments to the west, into a detached ductile fold-and-thrust fan in the eastern autochthon, separated by the high-angle Gourzy transfer fault. The rheology of the Paleozoic basement underlying the upper Cretaceous is key to this abrupt change in the deformation style. While the Eaux-Chaudes granite leads the localization of deformation

on top of it, placing the recumbent fold nappe, the eastern upper Paleozoic metasediments (Devonian limestones and schists) spread the deformation all over the stratigraphic pile including the upper Cretaceous.

There is no evidence of autochthonous Keuper remnants in between the Paleozoic basement and the Cretaceous rocks of the Eaux-Chaudes massif, but an allochthonous Keuper sheet emplaced on the upper Cretaceous by the Lower Lakora thrust in the beginning of the Pyrenean tectonic inversion, facilitated an upper detachment of the structure and the tightening of the recumbent fold. Detachment in Silurian slates was also instrumental in the development of the Eaux-Chaudes tight fold structure, allowing the upper Paleozoic to be entrained in the fold nappe core. Detachment in the Silurian is also inferred for the basement-involved thrust sheets that overlie the Eaux-Chaudes structure (Montagnon d'Iseye, Montagne Verte, Cinq Monts). Small intra-Cretaceous detachments and along the unconformity with the Paleozoic metasediments enhanced the shearing within the large-scale.

Unusual tertiary weld-like structures, marked by ophite and claystone/cargneule pinched slivers, attest for the allochthonous Keuper sheet. Unlike common tertiary welds, these are not localized between the subsalt and suprasalt rocks, but within tight synforms of the upper Cretaceous subsalt rocks, from which the bulk of the salt sheet was expelled. Weld-like structures also formed where slivers of the allochthonous Keuper sheet were pinched along former normal faults during their inversion.

Not only the western Eaux-Chaudes nappe conforms to a large recumbent fold evidencing Alpine ductile deformation in this segment of the Pyrenean hinterland, but also the Paleozoic basement units of Cinq Monts and Montagnon d'Iseye show

moderately large, overturned limbs delineated by post-Variscan, lower Triassic rocks. The deformation observed is consistent with the moderate paleotemperatures recorded in the post-Paleozoic rocks (300-360ºC) (Caldera et al., 2021). The nappe stacking at Eaux-Chaudes and surroundings represents a tectonic style not reported hitherto in the Alpine Pyrenees, evidencing relatively deep burial and/or high inherited thermal gradients during deformation, and basement-involved thin-skinned thrusting. This tectonic style characterizes the inversion of the previous Cretaceous rift during the early stages of the Pyrenean orogeny, at variance to the thick-skinned fan which structured the Axial Zone of the central Pyrenees during the subsequent fully-developed continental collision. It also warns on so-far unperceived Alpine ductile deformation in the basement of the Pyrenean hinterland.

ACKNOWLEDGMENTS

This work was supported by the Spanish MINECO/MCIU projects CGL2014-54180 and PGC2018-093903-B-C21. We thank Laura Burrel and Xavier Coll for assistance in the field, and Stéphane Dominguez for helpful discussions in the lab. Petroleum Experts is acknowledged for the permission to use the Move software via an academic license.

DATA AVAILABILITY STATEMENT

Further data that support the conclusions of this study are available from the corresponding author upon request.

REFERENCES CITED

778 Aerden, D. G. A. M. & Malavieille, J. (1999). Origin of a large-scale fold nappe in the
779 Montagne Noire, Variscan belt, France. *Journal of Structural Geology, 21 (10)*,
780 1321-1333. https://doi.org/10.1016/S01991-8141(99)00098-X
781 Alhamawi, M. (1992). Sédimentologie, pétrographie sédimentaire et diagenèse des
782 Calcaires du Crétacé supérieur de la Marge Ibérique : Bordeaux 1, 356 p.
783 Bastida, F. Aller, J., Fernández, F. J., Lisle, R. J., Bobillo-Ares, N. C. & Menéndez, O.
784 (2014). Recumbent folds: Key structural elements in orogenic belts. *Earth-Science*
785 *Reviews, 135*, 162-183. https://doi.org/10.1016/j.earscirev.2014.05.002
786 Bellahsen, N., Bayet, L., Denele, Y., Waldner, M., Airaghi, L., Rosenberg, C., Dubacq,
787 B., Mouthereau, F., Bernet, M., Pik, R., Lahfid, A. & Vacherat, A. (2019). Shortening
788 of the axial zone, Pyrenees: Shortening sequence, upper crustal mylonites and
789 crustal strength. *Tectonophysics, 766*, 433-452.
790 https://doi.org/10.1016/j.tecto.2019.06.002
791 Biteau, J. -J., Le Marrec, A., Le Vot, M. & Masset, J. -M. (2006). The Aquitaine Basin.
792 *Petroleum Geosciences, 12 (3)*, 247-273. https://doi.org/10.1144/1354-079305-674
793 Bosch, G., Teixell, A., Jolive, M., Labaume, P., Stockli, D., Domènech, M. & Monié, P.
794 (2016). Timing of Eocene-Miocene thrust activity in the Western Axial Zone and
795 Chaînons Béarnais (west-central Pyrenees) revealed by multi-method
796 thermochronology. *Comp. Rendus Geosci. 348*, 246-256.
797 https://doi.org/10.1016/j.crte.2016.01.001
798 Bresson, A. (1903). Étude sur les formations anciennes des Hautes et Basses-
799 Pyrénées (Haute-Chaîne). *Bull. Serv. Carte géol. Fr., 93 (14),* 278 p.

Bresson, A. (1906). Réunion extraordinaire de la Société Géologique de France dans les Pyrénées occidentales en 1906. *Bulletin Societé Géologique France, 4º série*, t. VI, 777-884.

Butler, R. W. H., Tavarnelli, E. & Grasso, M. (2006). Structural inheritance in mountain belts: An Alpine-Apennine perspective. *Journal of Structural Geology, 28 (11)*, 1893-1908. https://doi.org/10.1016/j.jsg.2006.09.006

Caldera, N., Teixell, A., Griera, A., Labaume, P. & Lahfid, A. (2021). Recumbent folding in the Upper Cretaceous Eaux-Chaudes massif: A Helvetic-type nappe in the Pyrenees?. *Terra Nova, 33,* 320-331. https://doi.org/10.1111/ter.12517

Casteras, M. (1956). Calcaire des Eaux-Chaudes (France, Basses, Pyrénées) – Garumnien – Poudingue de Mendibelza. *In Lexique stratigraphique international, 1*, 4a VI, Crétacé.

Casteras, M. & Souquet, P. (1964). Sur la constitution et sur la structure de la couverture crétacée de la Zone primaire axiale pyrénéenne à l'Ouest du Pic d'Anie. *C. R. Acad. Sc.*, Paris, 259 (17), 2881-2886.

Chevrot, S., Sylvander, M. Diaz, J., Martin, R., Mouthereau, F., Manatschal, G., Masini, E., Calassou, S., Grimaud, F., Pauchet, H. & Ruiz, M. (2018). The non-cylindrical crustal architecture of the Pyrenees. *Sci. Rep, 8*, 9591. https://doi.org/10.1038/s41598-018-27889-x

Clerc, C. & Lagabrielle, Y. (2014). Thermal control on the modes of crustal thinning leading to mantle exhumation: Insights from the Cretaceous Pyrenean hot paleomargins. *Tectonics, 33*, 1340-1359. https://doi.org/10.1002/2013TC003471

822 Clerc, C., Lahfid, A., Monié, P., Lagabrielle, Y., Chopin, C., Poujol, M., Boulvais, P.,
823 Ringenbach, J. -C., Masini, E. & de St. Blanquat, M. (2015). High-temperature
824 metamorphism during extreme thinning of the continental crust: a reappraisal of the
825 North Pyrenean passive paleomargin. *Solid Earth, 6, (2),* 643-668.
826 https://doi.org/10.5194/se-6-643-2015
827 Cochelin, B., Chardon, D., Denèle, Y., Gumiaux, C. & Le Bayon, B. (2017). Vertical
828 strain partitioning in hot Variscan crust: Syn-convergence escape of the Pyrenees in
829 the Iberian-Armorican syntax. *Bulletin de la Société Géologique de France, 188*, 39.
830 https://doi.org/10.1051/bsgf/2017026
831 Cochelin, B., Lemirre, B., Denèle, Y. & de Saint Blanquart, M. (2021). Strain partitioning
832 within bending orogens, new insights from the Variscan belt (Chilouret-Lesponne
833 domes, Pyrenees). *Tectonis, 40*, e2020TC006386.
834 https://doi.org/10.1029/2020TC006386
835 Conard, M. & Rioult, M. (1977). *Halimeda elliotti* nov. sp., Algue calcaire
836 (chlorophyceae) du Turonien des Alpes-Maritimes (Sud-Est de la France). *Géol.*
837 *Mèditer., 4, 2*, 43-72.
838 Curry, M. E., van der Beek, P., Huismans, R. S., Wolf, S. G., Fillon, C., Muñoz, J.-A.
839 (2021). Spatio-temporal patterns of Pyrenean exhumation revealed by inverse
840 thermos-kinematic modelling of a large thermochronologic data set. *Geology, 49*
841 *(6)*, 738-742. https://doi.org/10.1130/G48687.1
842 Cuvillier, J., Henry, J., Ribis, R. & Villanova, M. (1964). Microfaunes cenomaniennes et
843 santoniennes dans les ‘calcaires des canons’ (Vallee d’Aspe, Sainte-Engrace,

Basses-Pyrenees). *Bulletin de la Société Géologique de France, S7-VI (2)*, 273-277. https://doi.org/10.2113/gssgfbull.S7-VI.2.273

Debon, F. (1976). Les Eaux-Chaudes (Pyrénées occidentales): nouvel exemple de massif granitoïde pyrénéen à structure zonée. 4e RAST, Paris, *Soc. Géol. Fr., 125*.

Debon, F. (1996). Pluton des Eaux-Chaudes In : Magmatisme hercynien. In : Barnolas A., Chiron, J. C. (eds) Synthèse géologique at géophysique des Pyrénées, vol. 1. BRGM-ITGE, Orléans-Madrid, p. 410.

Debroas, E. -J. (1987). Modèle de basin triangulaire à l'intersection de décrochements divergents pour le fossé albo-cénomanien de la Ballongue (zone nord-pyrénéenne, France). *Bulletin de la Société Géologique de France, III*, 887-898.

Debroas, E. -J. (1990). Le Flysch noir albo-cénomanien témoin de la structuration albienne à sénonienne de la Zone nord-pyrénéenne en Bigorre (Hautes-Pyrénées, France). *Bulletin de la Société Géologique de France, VI*, 273-285.

Delvolvé, J. J. (1987). Un basin synorogénique varisque: le Culm des Pyrénées centro-occidentales. Thèse Doct. Sci., Toulouse, 483 p.

Déramond, J., Graham, R., Hossack, H., Baby, J. R., Crouzet, P. & Crouzet, G. (1985). Nouveau modéle de la chaîne des Pyrénées. *Comptes Rendus de l'Académie des Sciences, Paris, 301*, 1213-1216.

Ducoux, M., Jolivet, L., Masini, E., Augier, R., Lahfid, A., Bernet, M. & Calassou, S. (2021). Distribution and intensity of High-Temperature Low-Pressure metamorphism across the Pyrenean-Cantabrian belt: constraints on the thermal record of the pre-orogenic hyperextension rifting. *Bulletin de la Societé Géologique de France, 192 (1),* 43. https://doi.org/10.1051/bsgf/2021029

867 Dumont, T., Replumaz, A., Rouméjon, S., Briais, A., Rigo, A. & Bouillin, J.-P. (2015).
868 Microseismicity of the Béarn range: Reactivation of inversion and collision
869 structures at the northern edge of the Iberian plate. *Tectonics, 34*, 934-950.
870 https://doi.org/10.1002/2014TC003816
871 Espurt, N., Angrand, P., Teixell, A., Labaume, P., Ford, M., de Saint Blanquart, M. &
872 Chevrot, S. (2019). Crustal-scale balanced cross-section and restoration of the
873 Central Pyrenean belt (Nestes-Cinca transect): highlighting the structural control of
874 Variscan belt and Permian-Mesozoic rift systems on mountains building.
875 *Tectonophysics, 764*, 25-45. https://doi.org/10.1016/j.tecto.2019.04.026
876 Floquet, M., Mathey, B., Rosse, P. & Vadot, J. P. (1988). Age cenomanien et turono-
877 coniacien des calcaires de Sare (Pays Basque, France-Espagne); consequences
878 paleomorphologiques et tectogenetiques pour les Pyrenees occidentales. *Bulletin*
879 *de la Société Géologique de France, IV (6)*, 1021-1027.
880 https://doi.org/10.2113/gssgfbull.IV.6.1021
881 Ford, M., Hemmer, L., Vacherat, A., Gallagher, K. & Christophoul, F. (2016). Retro-
882 wedge foreland basin evolution along the ECORS line, eastern Pyrenees, France.
883 *Journal of the Geological Society of London, 173*, 419-437.
884 https://doi.org/10.1144/jgs2015-129
885 Ford, M., Masini, E., Vergés, J., Pik, R., Ternois, S., Léger, J., Dielforder, A., Frasca, G.,
886 Grool, A., Vinciguerra, C., Bernard, T., Angrand, P., Crémades, A., Manatschal, G.,
887 Chevrot, S., Jolivet, L., Mouthereau, F., Thinon, I. & Calassou, S. (2022). Evolution
888 of a low convergence collisional orogen: a review of Pyrenean orogenesis. *Bulletin*

de la Société Géologique de France, 193 *(1)*, 19. https://doi.org/10.1051/bsgf/2022018

Fournier, E. (1905). Etudes géologiques sur la partie occidentale de la chaîne des Pyrénées, entre la vallée d'Aspe et celle de la Nieve. *Bulletin de la Société Géologique de la France*, *5*, 699-723.

García-Sansegundo, J., Poblet, J., Alonso, J. L. & Clariana, P. (2011). Hinterland-foreland zonation of the Variscan orogen in the Central Pyrenees: Comparison with the northern part of the Iberian Variscan massif. *Geological Society, London, Special Publications, 349 (1),* 169-184. https://doi.org/10.1144/sp349.9

García-Senz, J., Pedrera, A., Ayala, C., Ruiz-Constán, A., Robador, A. & Rodríguez-Fernández, L. R. (2019). Inversion of the north Iberian hyperextended margin: the role of exhumed mantle indentation during continental collision. In: Hammerstein, J. A. (Ed.), Fold and Thrust Belts: Structural Style, Evolution and Exploration. *Geol. Soc.*, London, Spec. Publ, pp. 490. https://doi.org/10.1144/SP490-2019-112

Golberg, J. M. (1987). Le métamorphisme mésozoique dans la partie orientale des Pyrénées: relations avec l'évolution de la chaîne au Crétacé. Doc. Trav. Centre Géol Geophys Montpellier 14: 235 p.

Golberg, J. M. & Leyreloup, A. F. (1990). High temperature-low pressure Cretaceous metamorphism related to crustal thinning (Eastern North Pyrenean Zone, France). *Contributions to Mineralogy and Petrology, 104*, 194-207. https://doi.org/10.1007/BF00306443

Grool, A. R., Ford, M., Vergés, J., Huismans, R. S., Christophoul, F. & Dielforder, A. (2018). Insights into the crustal-scale dynamics of a doubly vergente orogen from a

quantitative analysis of its forelands: a case study of the Eastern Pyrenees. *Tectonics, 37*, 450-476. https://doi.org/10.1002/2017TC004731

Guardia, M., Griera, A., Kaus, B., Piccolo, A., & Teixelll, A. (2020). Mechanical controls on recumbent folding from 2D numerical simulations. Applications to the Eaux-Chaudes fold nappe (west-central Pyrenees), *EGU General Assembly 2020*, Online, 4–8 May 2020, EGU2020-13505, https://doi.org/10.5194/egusphere-egu2020-13505

Guerrot, C. (2001). Datation du pluton des Eaux-Chaudes. In: Ternet, Y., Majesté-Menjoulas, C., Canérot, J., Baudin, T., Cocherie, A., Guerrot, C., Rossi, P. (eds) (2004). Notice explicative, Carte géol. France (1/50.000), feuille Laruns-Somport (1069). BRGM, Orléans, pp 185-187.

Izquierdo-Llavall, E., Román-Berdiel, T., Casas, A. M., Oliva-Urcia, B., Gil-Peña, I., Soto, R. & Jabaloy, A. (2012). Magnetic and structural study of the Eaux-Chaudes instrusion: understanding the Variscan deformation in the Western Axial Zone (Pyrenees). *Int. J. Earth Sci. (Geol. Rundsch), 101,* 1817-1834. https://doi.org/10.1007/s00531-012-0760-9

Jackson, M. & Hudec, M. (2017). Salt Tectonics: Principles and Practice. *Cambridge University Press*. https://doi.org/10.1017/9781139003988

Jammes, S., Manatschal, G., Lavier, L. & Masini, E. (2009). Tectonosedimentary evolution related to extreme crustal thinning ahead of a propagating ocean: Example of the western Pyrenees. *Tectonics, 28*, 1-24. https://doi.org/10.1029/2008TC002406

Jolivet, M., Labaume, P., Monié, P., Brunel, M., Arnaud, N. & Campani, M. (2007). Thermochronology constraints for the propagation sequence of the south Pyrenean basement thrust system (France-Spain). *Tectonics, 26 (5)*, 1-17. https://doi.org/10.1029/2006TC002080

Labaume, P., Meresse, F., Jolivet, M., Teixell, A. & Lahfid, A. (2016). Tectonothermal history of an exhumed thrust-sheet-top basin: An example from the south Pyrenean thrust belt. *Tectonics, 35*, 1280-1313. https://doi.org/10.1002/2016TC004192

Labaume, P. & Teixell, A. (2018). 3D structure of subsurface thrusts in the eastern Jaca Basin, southern Pyrenees. *Geol. Acta, 16*, 477-498. https://doi.org/10.1344/GeologicaActa2018.16.4.9

Labaume, P. & Teixell, A. (2020). Evolution of salt structures of the Pyrenean rift (Chaînons Béarnais, France): From hyper-extension to tectonic inversion. *Tectonophysics, 785*, 228451. https://doi.org/10.1016/j.tecto.2020.228451

Lacan, P. (2008). Activité Sismotectonique Plio-Quaternaire de l'Ouest des Pyrénées. Ph.D. Thesis, Université de Pau et des Pays de l'Adour, Pau. France.

Lacan, P. & Ortuño, M. (2012). Active tectonics of the Pyrenees: A review, *J. Iber. Geol., 38*, 9-30. https://doi.org/10.5209/rev_JIGE.2012.v38.n1.39203

Lagabrielle, Y. & Bodinier, J. L. (2008). Submarine reworking of exhumed subcontinental mantle rocks: Field evidence from the Lherz peridotites, French Pyrenees. *Terra Nova, 20 (1)*, 11-21. https://doi.org/10.1111/j.1365-3121.2007.00781.x

Lagabrielle, Y., Labaume, P. & de Saint Blanquat, M. (2010). Mantle exhumation, crustal denudation, and gravity tectonics during Cretaceous rifting in the Pyrenean

realm (SW Europe): Insights from the geological setting of the lherzolite bodies. *Tectonics, 29*, 1-26. https://doi.org/10.1029/2009TC002588

Majesté-Menjoulas, C., (1968). Le Peléozoïque au Nord du synclinorium des Eaux-Chaudes (Pyrénées Atlantiques). Thèse Doct. 3^{e} cycle, Toulouse.

Manatschal, G., Chenin, P., Lescoutre, R., Miró, J., Cadenas, P., Saspiturry, N., Masini, E., Chevrot, S., Ford, M., Jolivet, L., Mouthereau, F., Thinon, I., Issautier, B. & Calassou, S. (2021). The role of inheritance in forming rifts and rifted margins and buildings collisional orogens: a Biscay-Pyrenean perspective. *Bulletin de la Société Géologique de France, 192 (1)*, 55. https://doi.org/10.1051/bsgf/2021042

Masini, E., Manatschal, G., Tugend, J., Mohn, G. & Flament, J.-M. (2014). The tectono-sedimentary evolution of a hyper-extended rift basin: The example of the Arzacq-Mauléon rift system (Western Pyrenees, SW France). *International Journal of Earth Sciences, 103*, 1569-1596. https://doi.org/10.1007/s00531-014-1023-8

Matte, P. 2002. Les plis hercyniens kilométriques couchés vers l'ouest-sudouest dans la région du pic du Midi d'Ossau-col du Somport (zone axiale des Pyrénées occidentales). *Comptes Rendús Géoscience, 334*, 773-779.

Mirouse, R. (1962). Recherches géologiques dans la partie occidentale de la zone primaire axiale des Pyrénées. Thèse État, Toulousse. *Mém. Serv. Carte géol. Fr. (1966),* 451 p. (Paris).

Mouthereau, F., Filleaudeau, P.-Y., Vacherat, A., Pik, R., Lacombe, O., Fellin, M. G., Castelltort, S., Christophoul, F. & Masini, E. (2014). Placing limits to shortening evolution in the Pyrenees: Role of margin architecture and implications for the

Iberia/Europe convergence. *Tectonics, 33*, 2283-2314. https://doi.org/10.1002/2014TC003663

Ortí, F., Pérez-López, A. & Salvany, J. M. (2017). Triassic evaporites of Iberia: Sedimentological and palaeogeographical implications for the western Neotethys evolution during the Middle Triassic-Earliest Jurassic. *Palaeogeography, Palaeoclimatology, Palaeoecology, 471*, 157-180. https://doi.org/10.1016/j.palaeo.2017.01.025

Passchier, C. W. (2001). Flanking structures. *Journal of Structural Geology, 23, (6-7)*, 951-962. https://doi.org/10.1016/S0191-8141(00)00166-8

Pfiffner, O. A. (2017). Thick-skinned and thin-skinned tectonics: A global perspective. *Geosciences, 7(3)*, 71. https://doi.org/10.3390/geosciences7030071

Puigdefàbregas, C. (1975). La sedimentación molásica en la cuenca de Jaca. Pirineos. 104: 1-188.

Puigdefàbregas, C. & Souquet, P. (1986). Tecto-sedimentary cycles and depositional sequences of the Mesozoic and Tertiary from the Pyrenees. *Tectonophysics, 129 (1-4)*, 173-203. https://doi.org/10.1016/0040-1951(86)90251-9

Razin, P. (1989). Evolution tecto-sédimentaire alpine des Pyrénées Basques à l'Ouest de la transformante de Pamplona (province du Labourd). Thèse Doctorat Université de Bordeaux III, Bordeaux, 464 p.

Roigé, M., Gómez-Gras, D., Remacha, E., Daza, R., Boya, S. (2016). Tectonic control on sediment sources in the Jaca basin (Middle and Upper Eocene of the South-Central Pyrenees). *Comptes Rendus Geosciences, 348*, 236-245. https://doi.org/10.1016/j.crte.2015.10.005

Saspiturry, N., Allanic, C., Serrano, O., Courrioux, G., Baudin, T., Le Bayon, B., Lahfid, A., Razin, P., Villasenor, A., Cevrot, S. & Issautier, B. (2022). Upper lithospheric transfer zones driving the non-cylindricity of the West-Pyrenean orogenic prism (Mauléon hyperextended basin). *Journal of Structural Geology, 156*, 104535. https://doi.org/10.1016/j.jsg.2022.104535

Séguret, M. 1972. Étude tectonique des nappes et séries décollées de la partie centrale du versant sud des Pyrénées. *Sér. Géol. Struct., vol 2,* Publications de l'Univ. des Sciences et Techniques du Languedoc, Montpellier, France.

Soto, J. I., Flinch, J. F. & Tari, G. (2017). Permo-Triassic Salt Provinces of Europe, North Africa and the Atlantic margins: Tectonics and hydrocarbon potential. Oxford: Elsevier, Print.

Souquet, P. (1967). Le Crétacé supérieur sud-pyrénéen en Catalogne, Aragon et Navarre. Thèse Doct. Sci., univ. Toulousse.

Stevaux, J. & Winnock, E. (1974). Les bassins du Trias et du Lias inférieur d'Aquitaine et leurs épisodes évaporitiques. *Bulletin de la Societé Géologique de France, S7, 16 (6)*, 679-695. https://doi.org/10.2113/gssgfbull.S7-XVI.6.679

Stevaux, J. & Zolnai, G. (1975). Les Olistostromes du Sud de l'Aquitaine dans la dynamique du Bassin. IXe Congrès International de Sédimentologie, Nice.

Teixell, A. (1993). Coupe géologique du massif d'Igountze: implications sur l'évolution structurale de la bordure sud de la Zone nord-pyrénéenne occidentale. *Comptes Rendus de l'Académie des Sciences, Paris, 316*, 1789-1796.

1023 Teixell, A. (1996). The Ansó transect of the southern Pyrenees: Basement and cover
1024 thrust geometries. *Journal of the Geological Society of London, 153*, 301-310.
1025 https://doi.org/10.1144/gsjgs.153.2.0301
1026 Teixell, A., Durney, D. W. & Arboleya, M. L. (2000). Stress and fluid control on
1027 décollement within competent limestone. *Journal of Structural Geology, 22*, 349-
1028 371. https://doi.org/10.1016/S0191-8141(99)00159-5
1029 Teixell, A., Labaume, P. & Lagabrielle, Y. (2016). The crustal evolution of the west-
1030 central Pyrenees revisited: Inferences from a new kinematic scenario. *Comptes*
1031 *Rendus – Geoscience, 348*, 257-267. https://doi.org/10.1016/j.crte.2015.10.010
1032 Teixell, A., Labaume, P., Ayarza, P., Espurt, N., de Saint Blanquart, M. & Lagabrielle, Y.
1033 (2018). Crustal structure and evolution of the Pyrenean-Cantabrian belt: A review
1034 and new interpretations from recent concepts and data. *Tectonophysics, 724-725*,
1035 149-170. https://doi.org/10.1016/j.tecto.2018.01.009
1036 Ternet, Y. (1965). Étude du synclinal complexe des Eaux-Chaudes (Basses-Pyrénées),
1037 *Thèse Doctorat 3º Cycle: Faculté des sciences de l'Université de Toulouse*, 332 p.
1038 Ternet, Y., Majeste-Menjoulas, C., Canérot, J., Baudin, T., Cocherie, A., Guerrot, C. &
1039 Rossi, P. (2004). *Carte géologique de la France:* Laruns-Somport. Bureau de
1040 Recherches Géologiques et Minières, scale 1:50.000, feuille nº1069.
1041 Ternois, S., Odlum, M., Ford, M., Pik, R., Stockli, D., Tibari, B., Vacherat, A. & Bernard,
1042 V. (2019). Thermochronological evidence of early orogènesis, eastern Pyrenees,
1043 France. *Tectonics, 38 (4)*, 1308-1336. https://doi.org/10.1029/2018TC005254
1044 Tugend, J., Manatschal, G., Kusznir, N. J., Masini, E., Mohn, G. & Thinon, L. (2014).
1045 Formation and deformation of hyperextended rift Systems: insights from rift

domain mapping in the Bay of Biscay-Pyrenees. *Tectonics, 33*, 1239-1276. https://doi.org/10.1002/2014TC003529

Wayne, D. M. & McCaig, A. M. (1998). Dating fluid-flow in shear zones: Rb-Sr and U-Pb studies of syntectonic veins in Néouvielle Massif, Pyrenees. In: Parnell, J. (ed). Dating and Duration of Fluid Flow and Fluid-Rock Interactions. *The Geological Society of London, 144 (Special Publications)*, 129-135. https://doi.org/10.1144/GSL.SP.1998.144.01.09

Figure captions

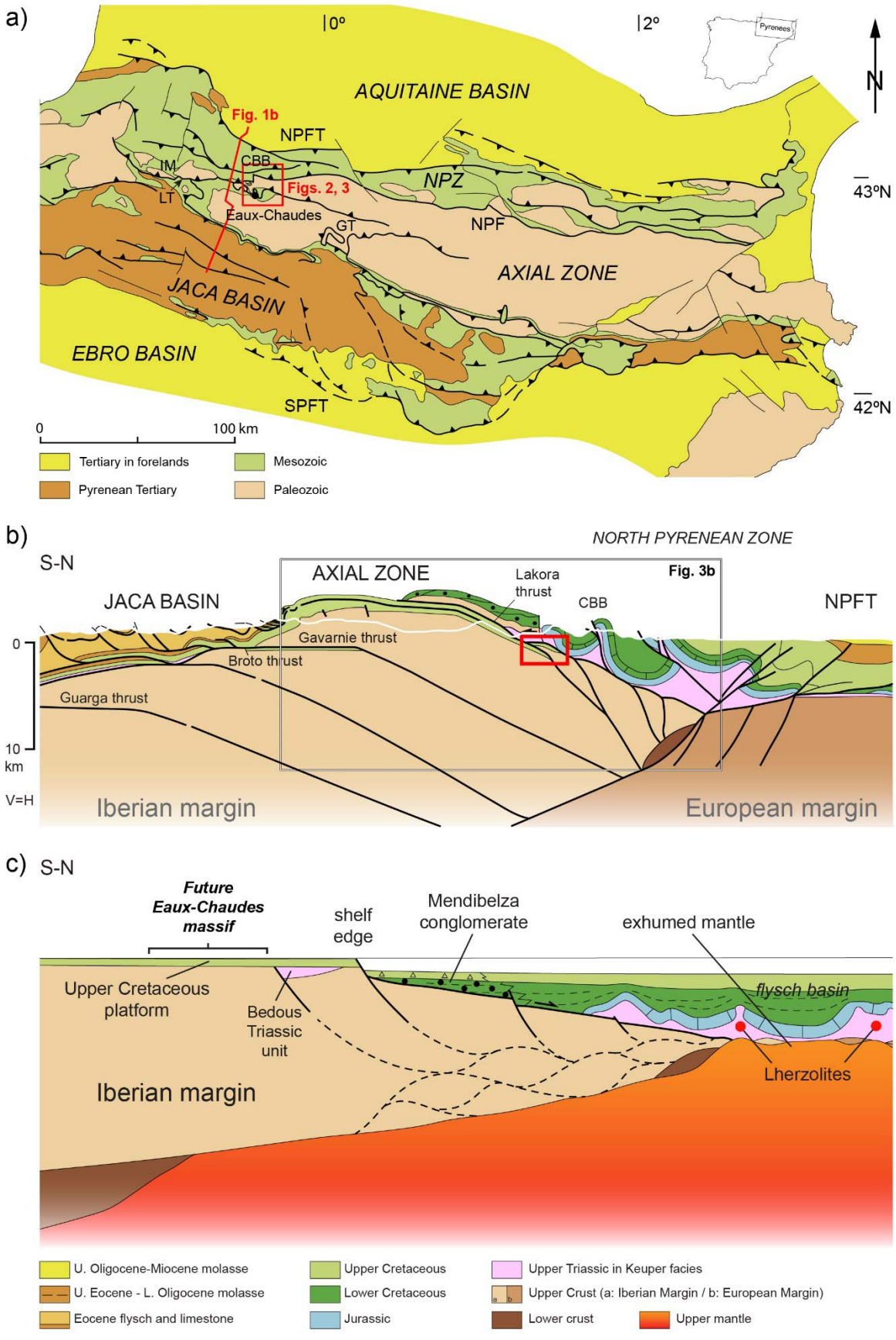
a)
|0°
|2°
Pyrenees
N
AQUITAINE BASIN
Fig. 1b
NPFT
CBB
IM
LT
Figs. 2, 3
NPZ
43°N
Eaux-Chaudes
GT
NPF
AXIAL ZONE
JACA BASIN
EBRO BASIN
SPFT
42°N
0
100 km
Tertiary in forelands
Mesozoic
Pyrenean Tertiary
Paleozoic
b)
NORTH PYRENEAN ZONE
S-N
AXIAL ZONE
Lakora thrust
Fig. 3b
JACA BASIN
CBB
NPFT
0
Gavarnie thrust
Broto thrust
Guarga thrust
10 km
V=H
Iberian margin
European margin
c)
S-N
Future Eaux-Chaudes massif
shelf edge
Mendibelza conglomerate
exhumed mantle
Upper Cretaceous platform
Bedous Triassic unit
flysch basin
Lherzolites
Iberian margin
U. Oligocene-Miocene molasse
U. Eocene - L. Oligocene molasse
Eocene flysch and limestone
Upper Cretaceous
Lower Cretaceous
Jurassic
Upper Triassic in Keuper facies
Upper Crust (a: Iberian Margin / b: European Margin)
Lower crust
Upper mantle

1056 **Fig.**

1. (a) Geologic sketch map of the Pyrenees showing the location of the Eaux-Chaudes massif. Red frame indicates the mapped area (Figs. 2, 3) and red line indicates cross-section in Fig. 1b. (b) Crustal cross-section of the Pyrenees west of the study area (simplified from Teixell et al., 2016) showing the tectonic setting of the Eaux-Chaudes structures (red frame). Black frame indicates the part of the section used to show the Lakora thrust system trace in Fig. 3b. (c) Restored crustal cross-section of the Iberian margin and rift axis to the Late Cretaceous (Santonian) from Fig. 1b (modified from Teixell et al., 2016). CBB: Chaînons Béarnais Belt; IM: Igountze and Mendibelza massifs; GT: Gavarnie thrust; LT: Lakora thrust; NPZ: North Pyrenean Zone; NPF: North Pyrenean Fault; NPFT: North Pyrenean Frontal thrust; SPFT: South Pyrenean Frontal thrust.

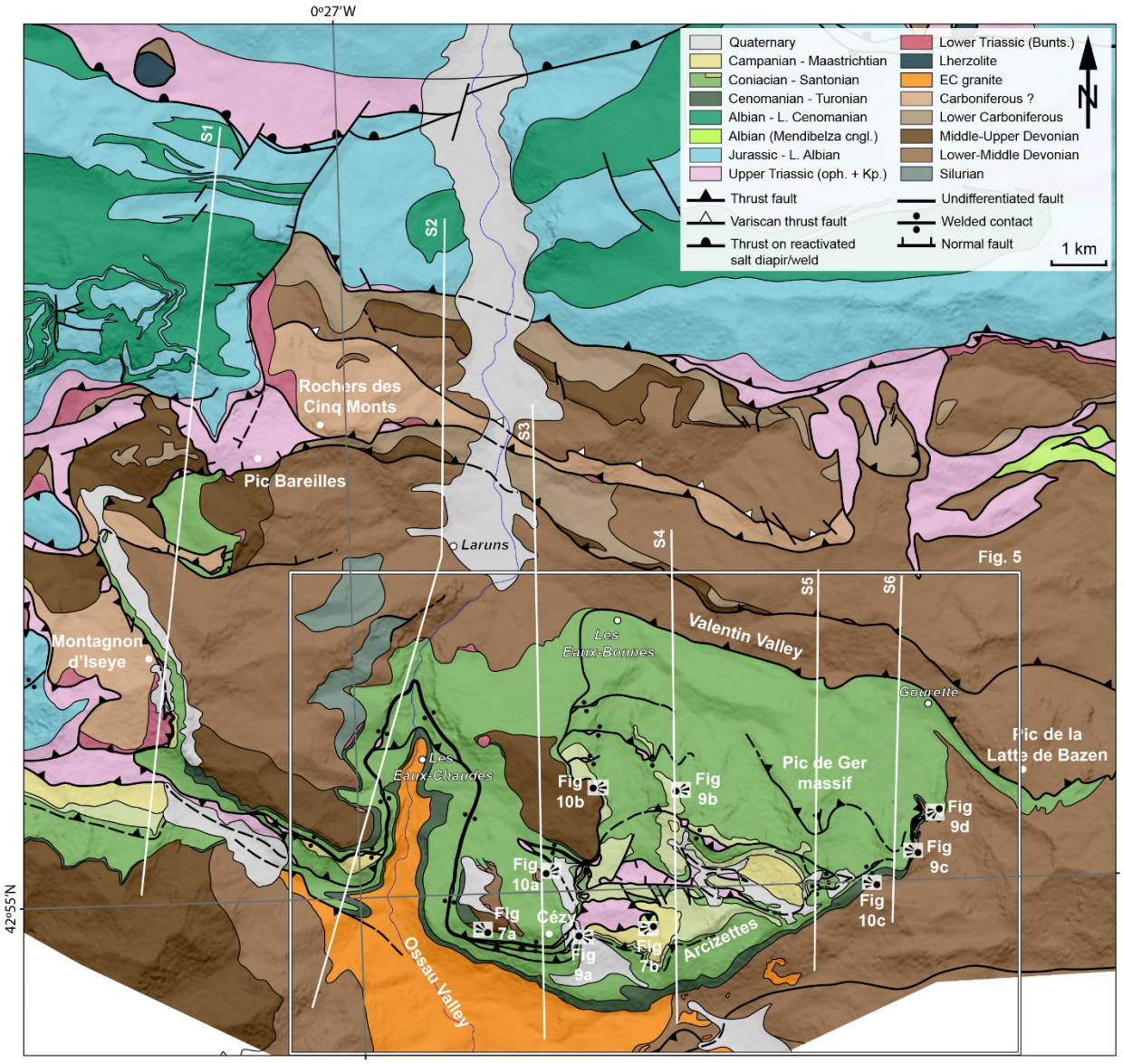

Fig. 2. Geological map of the Eaux-Chaudes massif and surrounding areas (location in Fig. 1a). Data compiled from published maps (Ternet, 1965; Ternet et al., 2004; Labaume & Teixell, 2020; Caldera et al., 2021), and own field observations. White frame indicates the mapped area amplified in Fig. 5. S1 to S3: cross-sections in Fig. 6. S4 to S6: cross-sections in Fig. 8. Indicated in the legend with a question mark is an azoic succession of limestones and slates attributed tentatively to the Carboniferous by Ternet et al. (2004) and labelled hCM in Fig. 4.

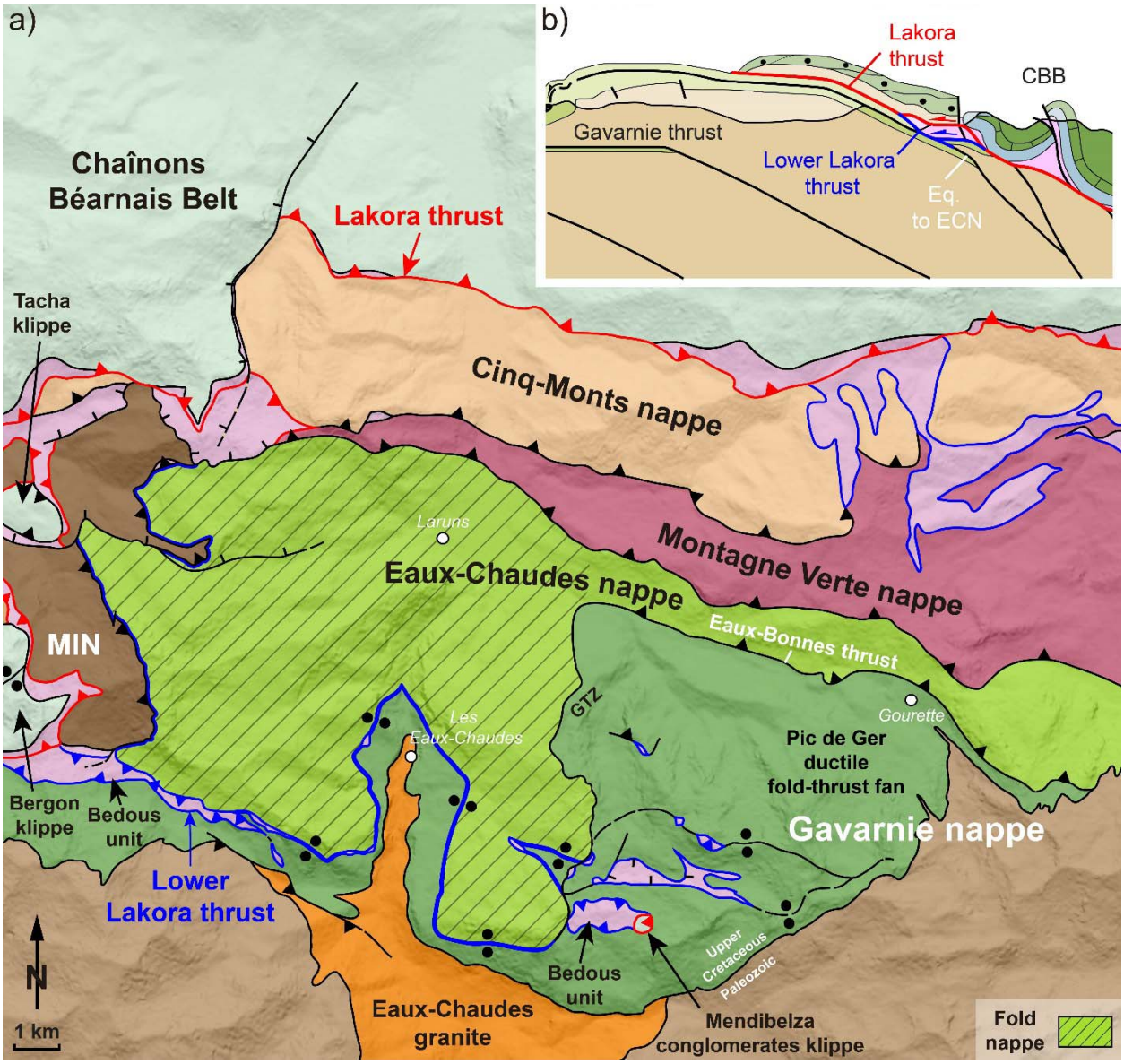

Fig. 3. (a) Simplified tectonic map of the Eaux-Chaudes massif and southern edge of the Chaînons Béarnais Belt showing the structural units referred to in the text. Bedous unit corresponds to the upper Triassic carried by the Lower Lakora thrust. MIN: Montagnon d'Iseye nappe; GTZ: Gourzy Transfer Zone. (b) Detail of the cross-section in Fig. 1b from the Gavarnie nappe and its overlying tectonic units indicating the structural position of the Lower Lakora thrust and Lakora thrust *s.s.*

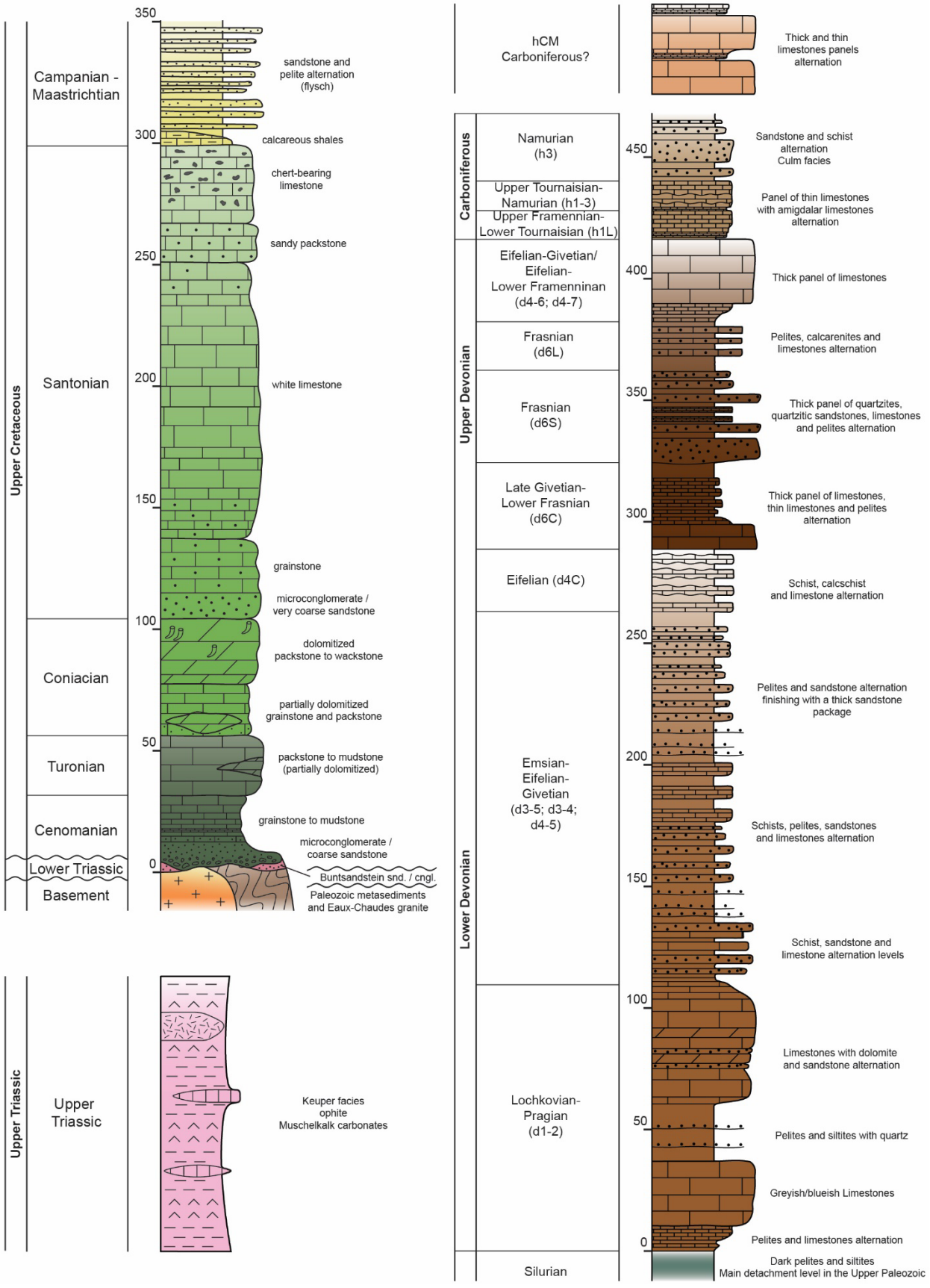
Upper Cretaceous
Campanian - Maastrichtian
Santonian
Coniacian
Turonian
Cenomanian
Lower Triassic
Basement
350
300
250
200
150
100
50
0
sandstone and pelite alternation (flysch)
calcareous shales
chert-bearing limestone
sandy packstone
white limestone
grainstone
microconglomerate / very coarse sandstone
dolomitized packstone to wackstone
partially dolomitized grainstone and packstone
packstone to mudstone (partially dolomitized)
grainstone to mudstone
microconglomerate / coarse sandstone
Buntsandstein snd. / cngl.
Paleozoic metasediments and Eaux-Chaudes granite
Upper Triassic
Upper Triassic
Keuper facies
ophite
Muschelkalk carbonates
hCM
Carboniferous?
Thick and thin limestones panels alternation
Carboniferous
Namurian (h3)
Upper Tournaisian-Namurian (h1-3)
Upper Framennian-Lower Tournaisian (h1L)
Upper Devonian
Eifelian-Givetian/ Eifelian-Lower Framenninan (d4-6; d4-7)
Frasnian (d6L)
Frasnian (d6S)
Late Givetian-Lower Frasnian (d6C)
Eifelian (d4C)
Lower Devonian
Emsian-Eifelian-Givetian (d3-5; d3-4; d4-5)
Lochkovian-Pragian (d1-2)
Silurian
450
400
350
300
250
200
150
100
50
0
Sandstone and schist alternation Culm facies
Panel of thin limestones with amigdalar limestones alternation
Thick panel of limestones
Pelites, calcarenites and limestones alternation
Thick panel of quartzites, quartzitic sandstones, limestones and pelites alternation
Thick panel of limestones, thin limestones and pelites alternation
Schist, calcschist and limestone alternation
Pelites and sandstone alternation finishing with a thick sandstone package
Schists, pelites, sandstones and limestones alternation
Schist, sandstone and limestone alternation levels
Limestones with dolomite and sandstone alternation
Pelites and siltites with quartz
Greyish/blueish Limestones
Pelites and limestones alternation
Dark pelites and siltites
Main detachment level in the Upper Paleozoic

Fig. 4. Simplified stratigraphic logs of the Paleozoic and Mesozoic of the Eaux-Chaudes massif (based on Ternet, 1965, and own data).

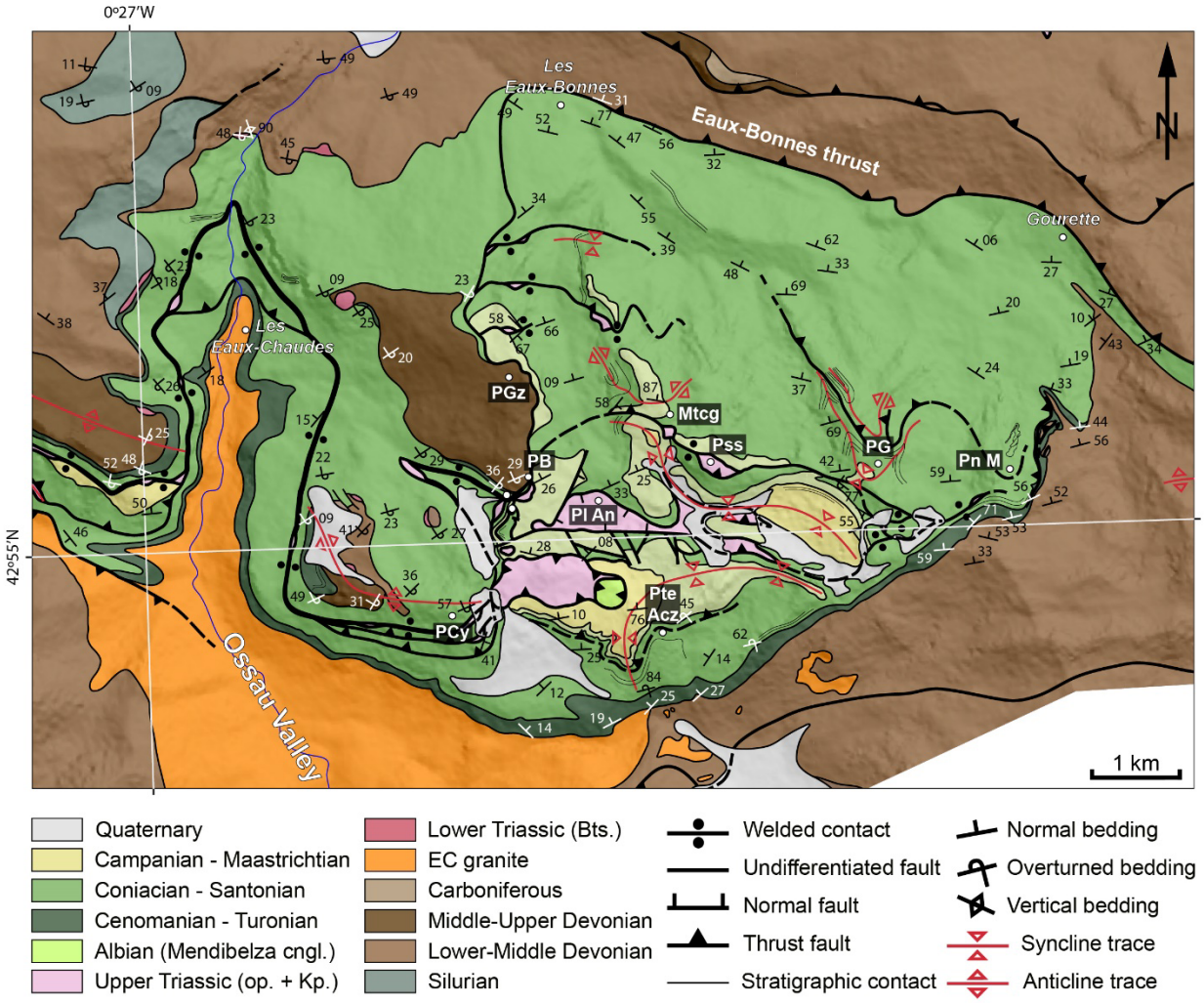

Fig. 5. Detailed geological map of the Eaux-Chaudes massif (from Fig. 2) showing structural data and the situation of the main localities referred to in the text. PCy: Pic de Cézy; PGz: Pic du Gourzy; PB: Pic de Brèque; Pl An: Plateau d'Anouilhas; Pte Acz: Petite Arcizette; Mtcg: Montcouges; Pss: Pambassibé; PG: Pic de Ger; Pn M: Pêne Médaa.

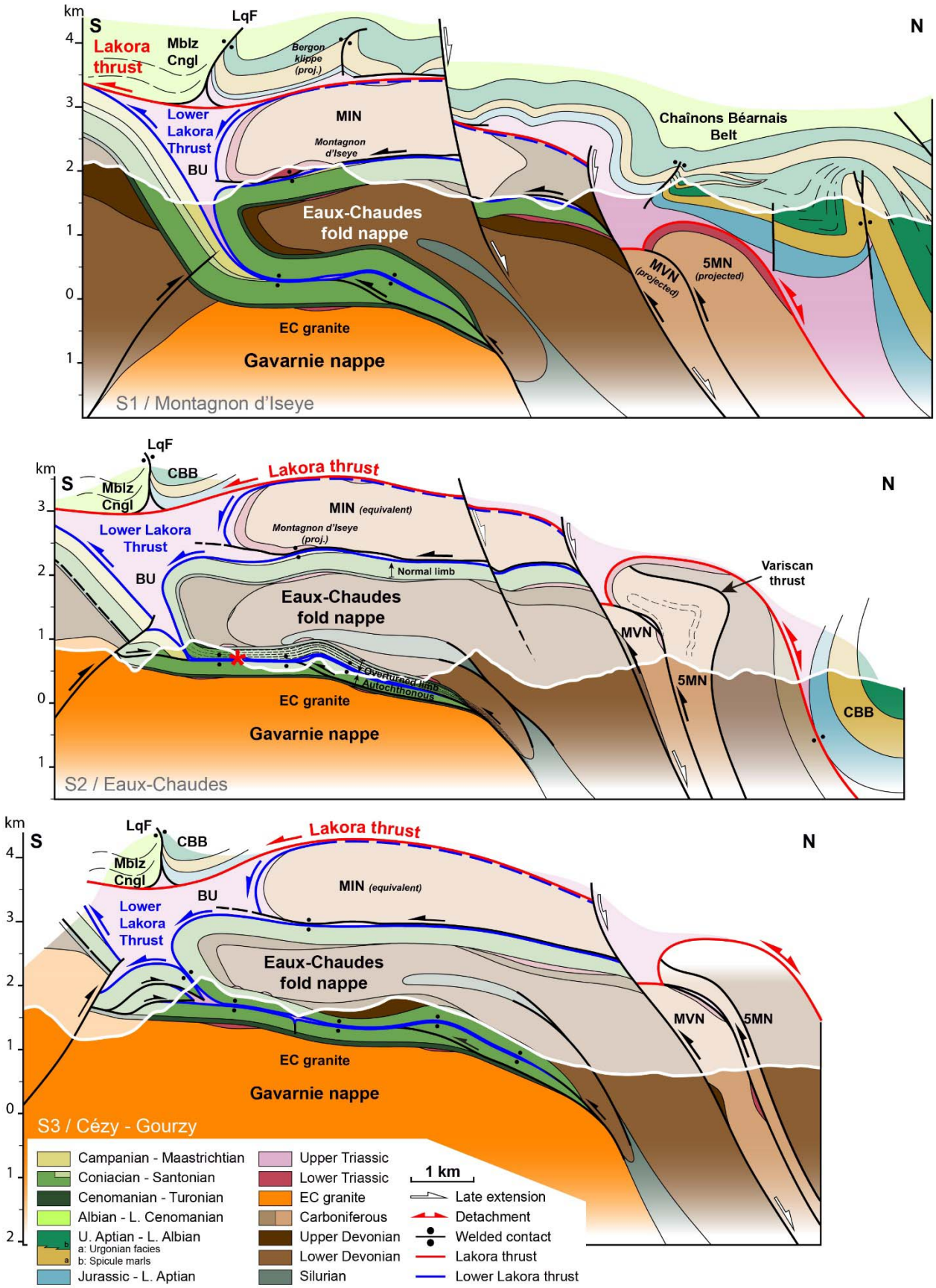
km
S
N
LqF
Lakora thrust
Mblz
Cngl
Bergon klippe (proj.)
Lower Lakora Thrust
BU
MIN
Montagnon d'Iseye
Chaînons Béarnais Belt
Eaux-Chaudes fold nappe
MVN (projected)
5MN (projected)
EC granite
Gavarnie nappe
S1 / Montagnon d'Iseye
CBB
MIN (equivalent)
Montagnon d'Iseye (proj.)
Normal limb
Variscan thrust
MVN
5MN
Overturned limb
Autochthonous
S2 / Eaux-Chaudes
S3 / Cézy - Gourzy
Campanian - Maastrichtian
Coniacian - Santonian
Cenomanian - Turonian
Albian - L. Cenomanian
U. Aptian - L. Albian
a: Urgonian facies
b: Spicule marls
Jurassic - L. Aptian
Upper Triassic
Lower Triassic
EC granite
Carboniferous
Upper Devonian
Lower Devonian
Silurian
1 km
Late extension
Detachment
Welded contact
Lakora thrust
Lower Lakora thrust

Fig. 6. Geological cross-sections of the western sector of the Eaux-Chaudes massif presenting the lateral variation of the Eaux-Chaudes unit from west to east (S1 – S3). See location in Fig. 2. Red asterisk in S2 shows the location of the allochthon Keuper pinched in the welded syncline of the recumbent fold, shown in Sup. 1. Mblz Cngl: Mendibelza Conglomerates; LqF: Licq Fault; MIN: Montagnon d'Iseye nappe; 5MN: Cinq Monts nappe; MVN: Montagne Verte nappe; CBB: Chaînons Béarnais Belt; BU: Bedous Unit (carried by the Lower Lakora thrust). Jurassic and Lower Cretaceous rocks of the CBB in section 1 are based on Labaume & Teixell, 2020.

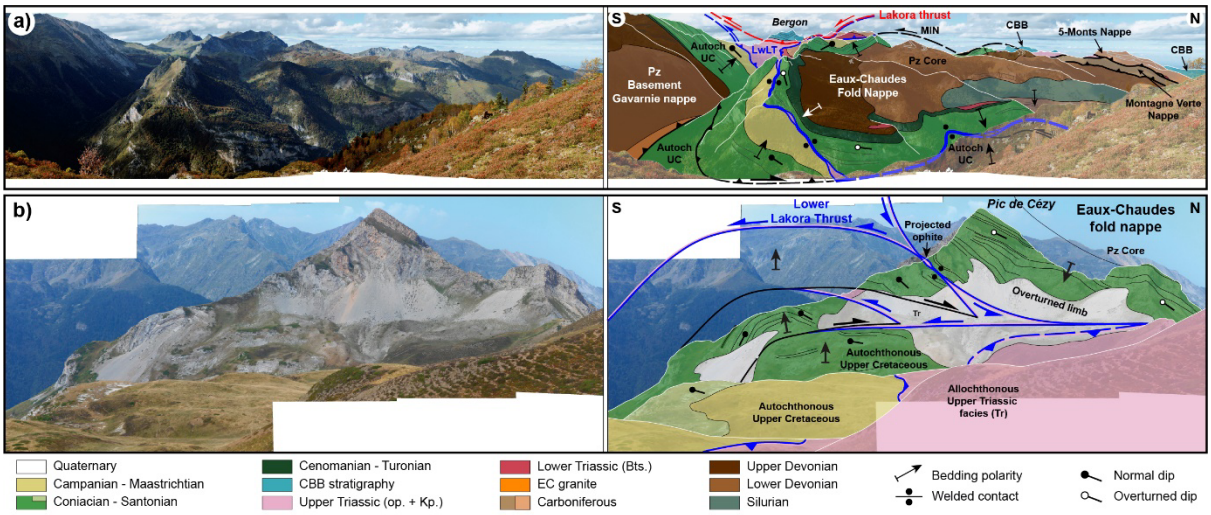

Fig. 7. Interpreted panoramas showing different examples of deformation in the upper Cretaceous of the western part of the Eaux-Chaudes massif (location of views in Fig. 2). (a) Interpreted panorama of the Eaux-Chaudes recumbent fold and overlying tectonic units (MIN, Lower Lakora and Lakora thrusts, 5MN, CBB, MVN; for explanation of acronyms, refer to the legend of the previous figure) in the Ossau Valley from an eastern viewpoint. It corresponds to the southern part of sections 1 and 2 (Fig. 6). (b) Interpreted panorama of the Pic de Cézy from an eastern viewpoint. It corresponds to the southern termination of the recumbent fold in section 3 (Fig. 6). The system of late backthrusts (black) overprints the Lower Lakora thrust (blue), which is marked by Keuper and ophite bodies.

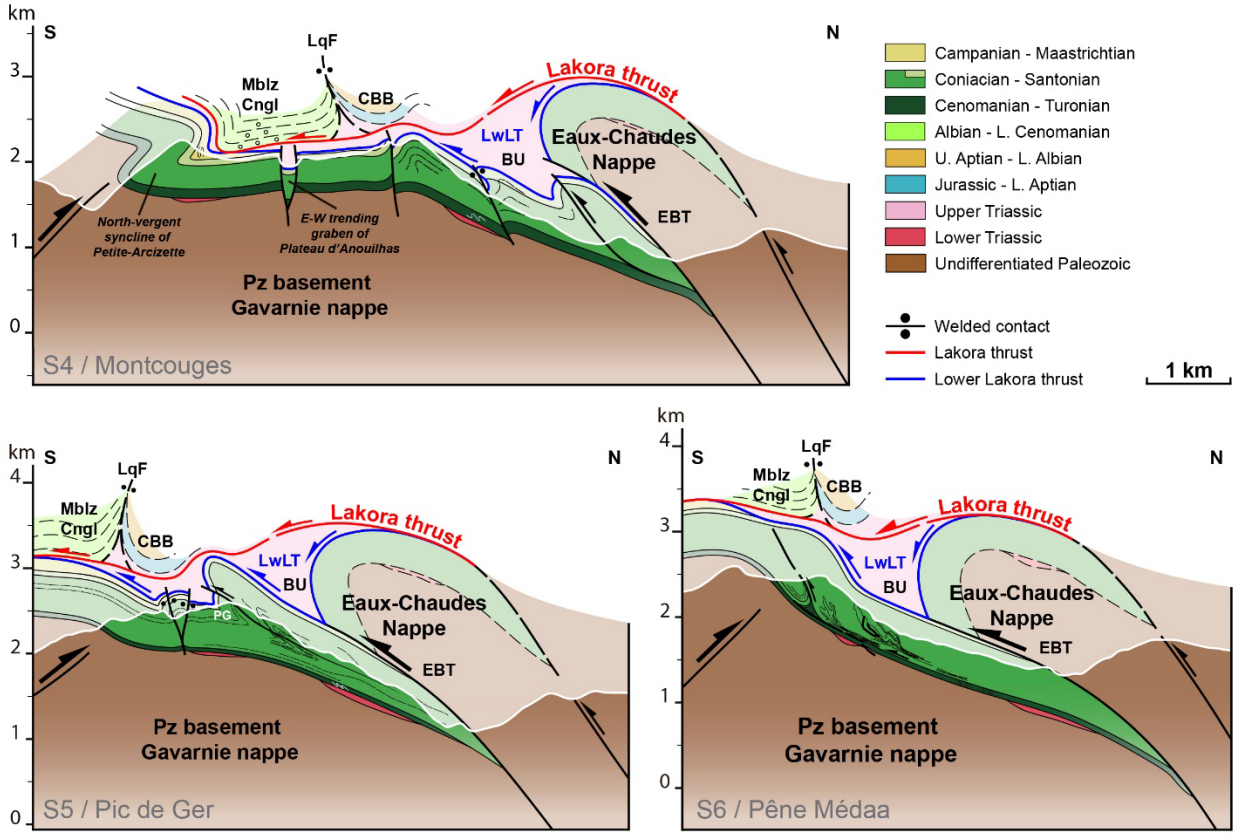

Fig. 8. Geological cross-sections of the eastern sector of the Eaux-Chaudes massif featuring the strong ductile deformation in the autochthonous upper Cretaceous. See location in Fig. 2. Mblz Cngl: Mendibelza Conglomerates; LqF: Licq Fault; CBB: Chaînons Béarnais Belt; LwLt: Lower Lakora thrust; BU: Bedous Unit (carried by the Lower Lakora thrust); EBT: Eaux-Bonnes Thrust; PG: Pic de Ger in S5. The Eaux-Chaudes fold nappe illustrated in sections in Fig. 6 is tentatively interpreted to be replaced in these transects by a simple thrust-related ramp anticline, whereas much of the deformation is transferred to its footwall.

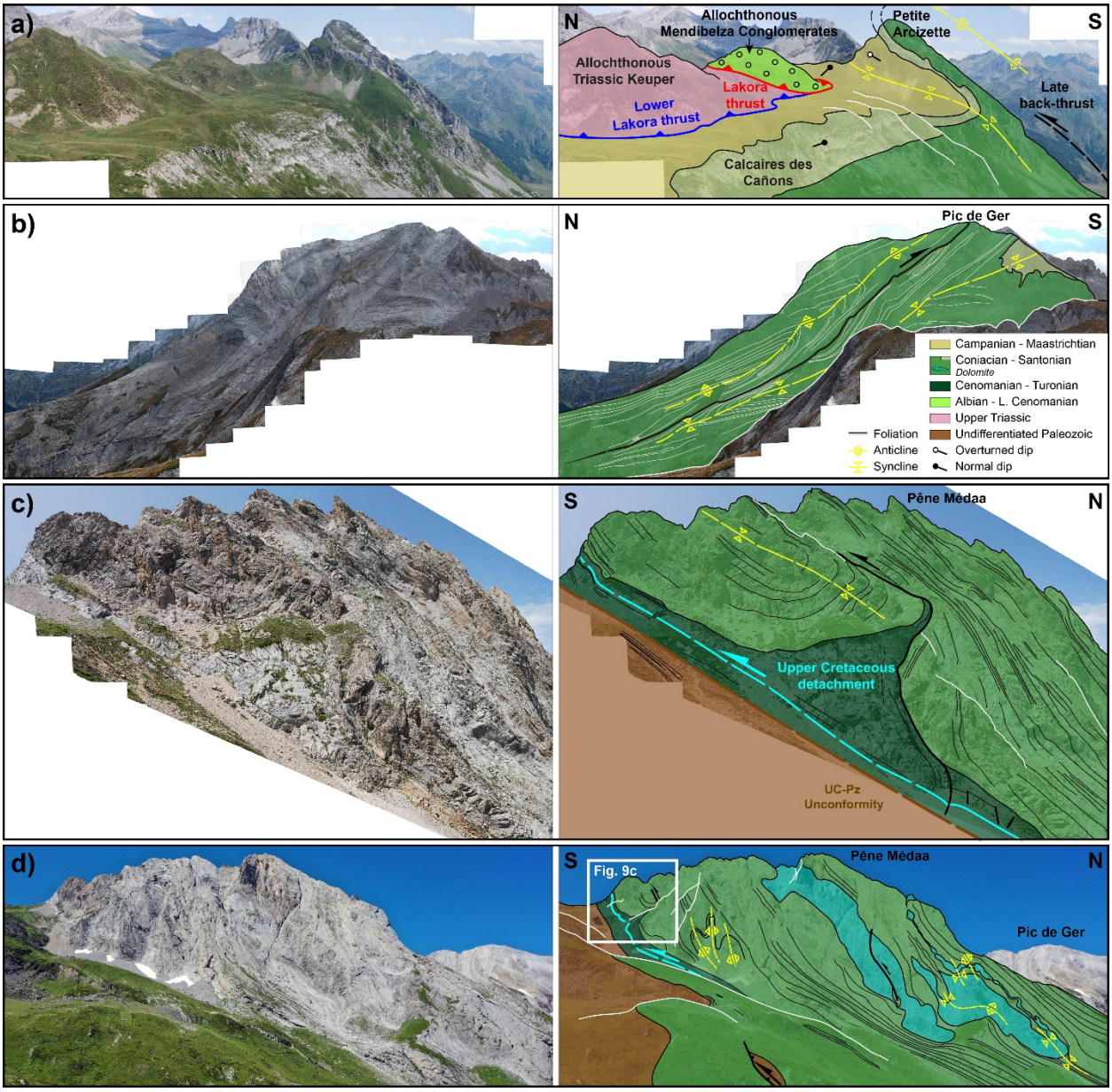

Fig. 9. Interpreted panoramas showing different examples of deformation in the upper Cretaceous of the eastern part of the Eaux-Chaudes massif (location of views in Fig. 2). (a) View from the west of the Petite Arcizette north-verging syncline. (b) View from the west of the Pic de Ger. A large-scale isoclinal anticline-syncline pair with an intervening thrust attests for a strong component of ductile deformation in the upper Cretaceous. A view of the syncline on the eastern slope of the Pic de Ger is in Fig. 10c. (c) View from the east of the Pêne Médaa showing an intra-Cretaceous detachment at the level of the Cenomanian. Ductile deformation

led to folding and squeezing of the lower limestone units. (d) View from the east of the northern slope of Pêne Médaa showing large-scale dolomitic bodies affected by boudinage, folds and thrusts evidencing intense deformation in this area. Widespread mylonitic foliation in the host limestones is indicated by black lines. Small thrusts affect the basal unconformity.

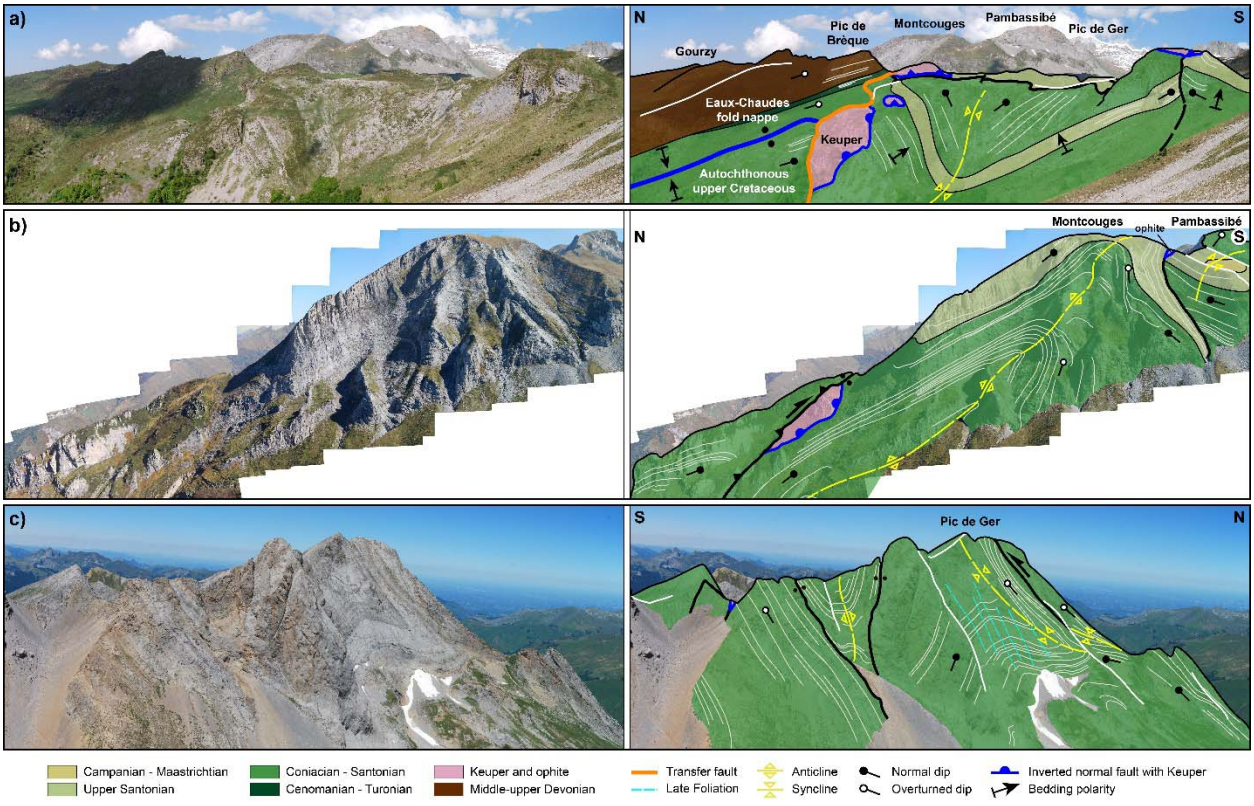

Fig. 10. Interpreted panoramas of salt weld-like structures in the eastern Eaux-Chaudes massif (see location of pictures in Fig. 2). Weld structures are marked by ophite or Keuper shale slivers enclosed in the upper Cretaceous limestone and were mapped originally by Ternet (1965), who interpreted them as squeezed diapiric structures coming from below. Here we interpret them as tertiary welds coming from the overlying, allochthonous Keuper sheet (Bedous unit, see text for explanation). (a) View from the west of the Pic de Brèque with the large ophite body in the autochthon of the Eaux-Chaudes fold nappe. The autochthon is deformed by the inversion of an extensional small graben which originally cut the Lower Lakora thrust (see text for explanation).

(b) View from the west of the Montcouges and Pambassibé mountains, showing a large, detached anticline limited to the north and south by former extensional faults tectonically inverted. Ophite rocks are pinched in faults, witnessing their compressional tightening. The tightening of the fold is accompanied by foliation in the carbonates. (c) View from the east of the Pic de Ger ridge showing the prominent syncline imaged in Fig. 9b and faulted contacts to the south that are marked by Triassic slivers. Strong ductility is evidenced by the penetrative mylonitic foliation which is folded by the syncline. A vertical foliation (blue dashed lines), which is oblique to the axial plane of the fold developed during a later deformation episode.

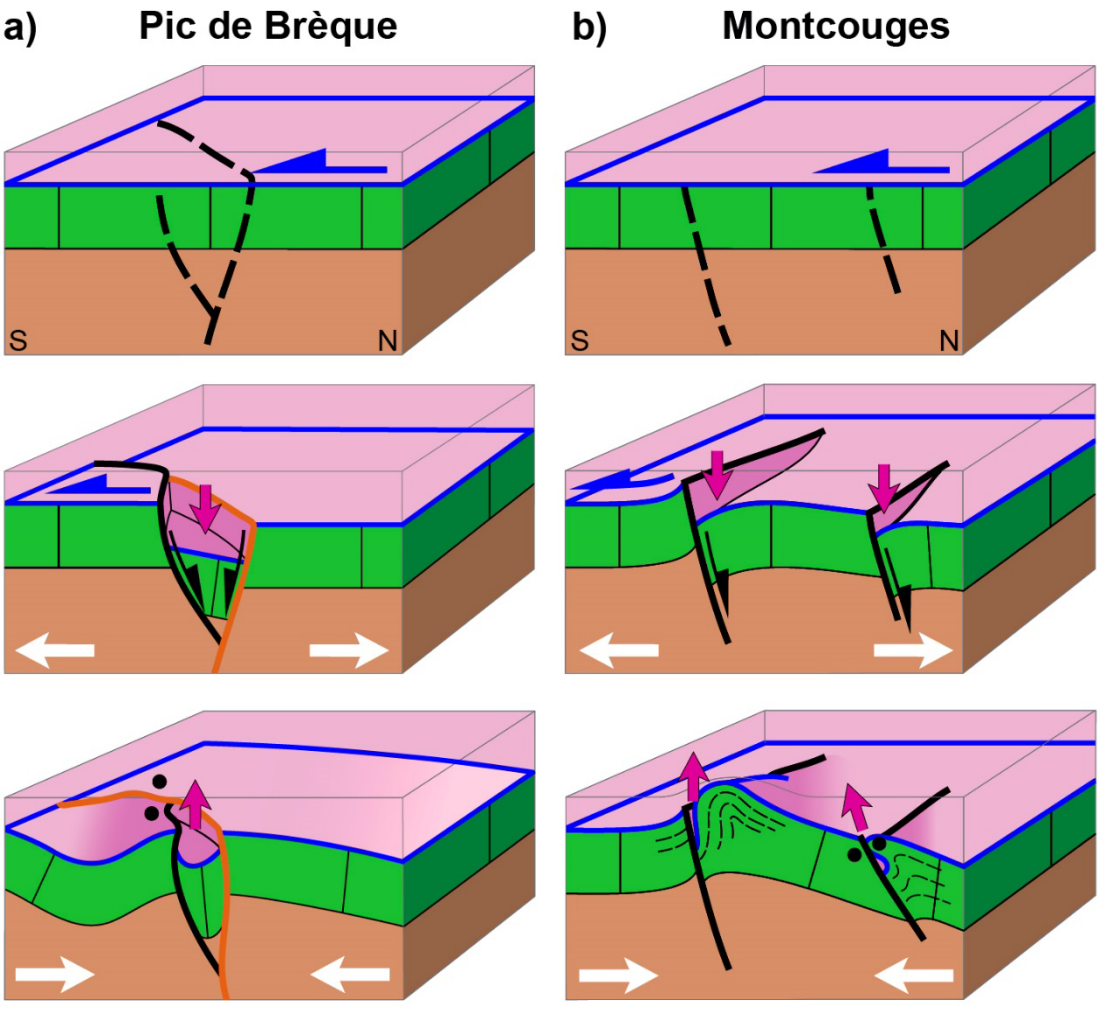

1158 **Fig. 11.** Cartoons explaining the occurrence of pinched Keuper and ophite bodies in the upper
1159 Cretaceous carbonates in two sections of the Eaux-Chaudes massif (cf. Fig. 5 for location and
1160 10 for illustration). In the first step the Lower Lakora thrust emplaced the allochthon Keuper
1161 sheet (Bedous unit) over the upper Cretaceous. In a second step, extensional structures were
1162 formed and/or enhanced inheritance reactivation by the flexure associated to the thrust load,
1163 resulting in the mobilisation of the Keuper rocks into depressed areas. Finally, in the shortening
1164 step, structures related with salt were welded when small bodies of upper Triassic got trapped in
1165 the core of the previous extensional structures and deformed by flattening and inversion. The
1166 overlying Eaux-Chaudes nappe and subsequent upper nappes are not represented to simplify
1167 the illustration. In a) orange line correspond to the Gourzy Transfer Zone.
1168

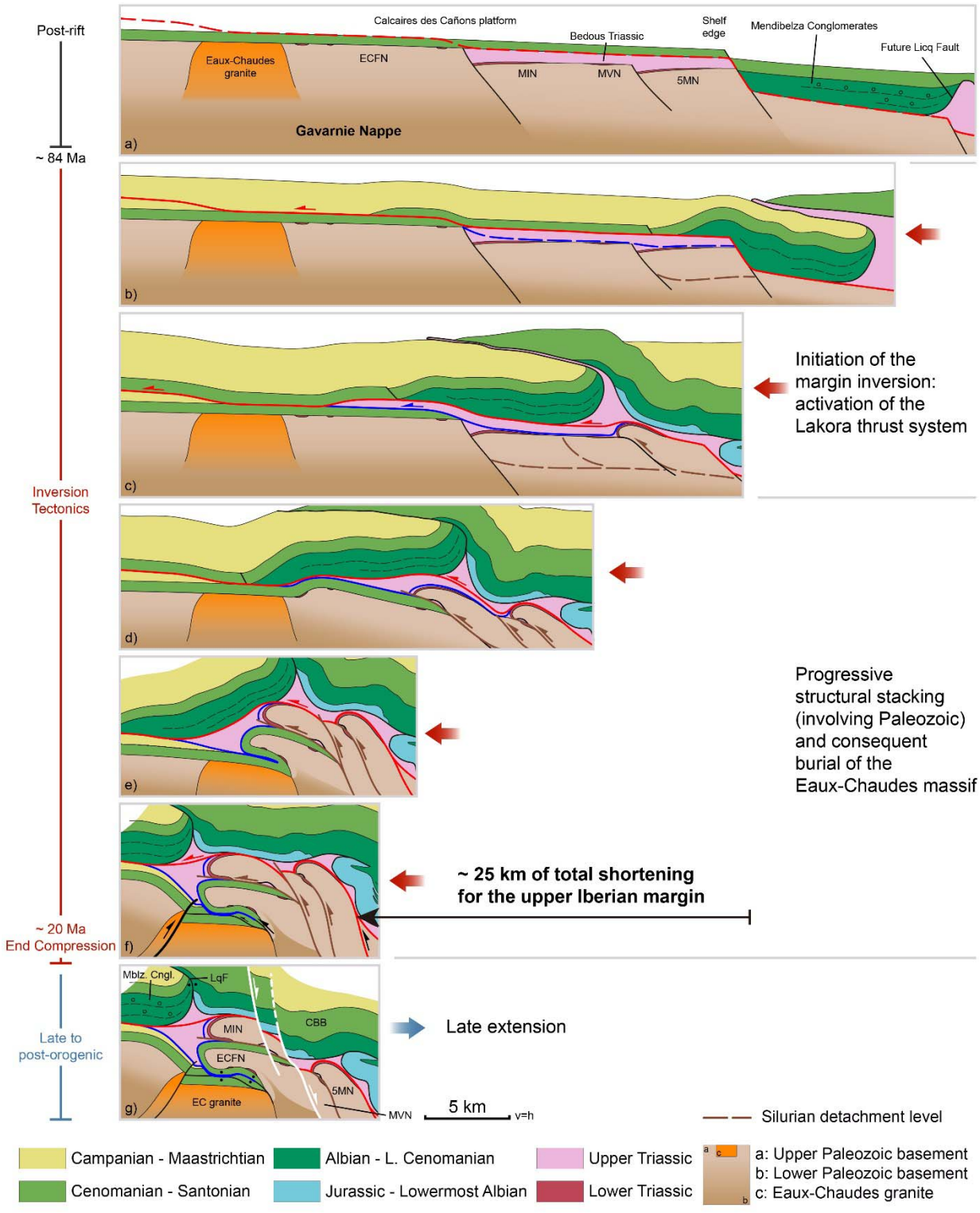

1169

1170 **Fig. 12.** Sketch illustrating the proposed sequence for the compressional inversion of the

1171 uppermost Iberian margin in the western Eaux-Chaudes massif, including the structural stacking

1172 of the upper thrust units. Red line corresponds to the Lakora thrust carrying the detached CBB

and Mendibelza conglomerates. Blue line corresponds to the lower branch of the Lakora thrust carrying the allochthonous Keuper sheet (horse) of the Bedous unit on the ECFN. Dashed lines show the location of future faults in the following steps. The structure of the pre-inversion stage (a) is modified from the model of hyper-extension of Teixell et al. (2016). The last stage (f) is based on the cross-sections S1 and S2 from Fig. 6 for the ECFN, MIN, 5MN and MVN. The kinematic evolution of the CBB is taken from Labaume & Teixell (2020). ECFN: Eaux-Chaudes fold nappe; MIN: Montagnon d'Iseye nappe; 5MN: 5 Monts nappe; MVN: Montagne Verte nappe; CBB: Chaînons Béarnais Belt; Mblz. Cngl: Mendibelza Conglomerates.

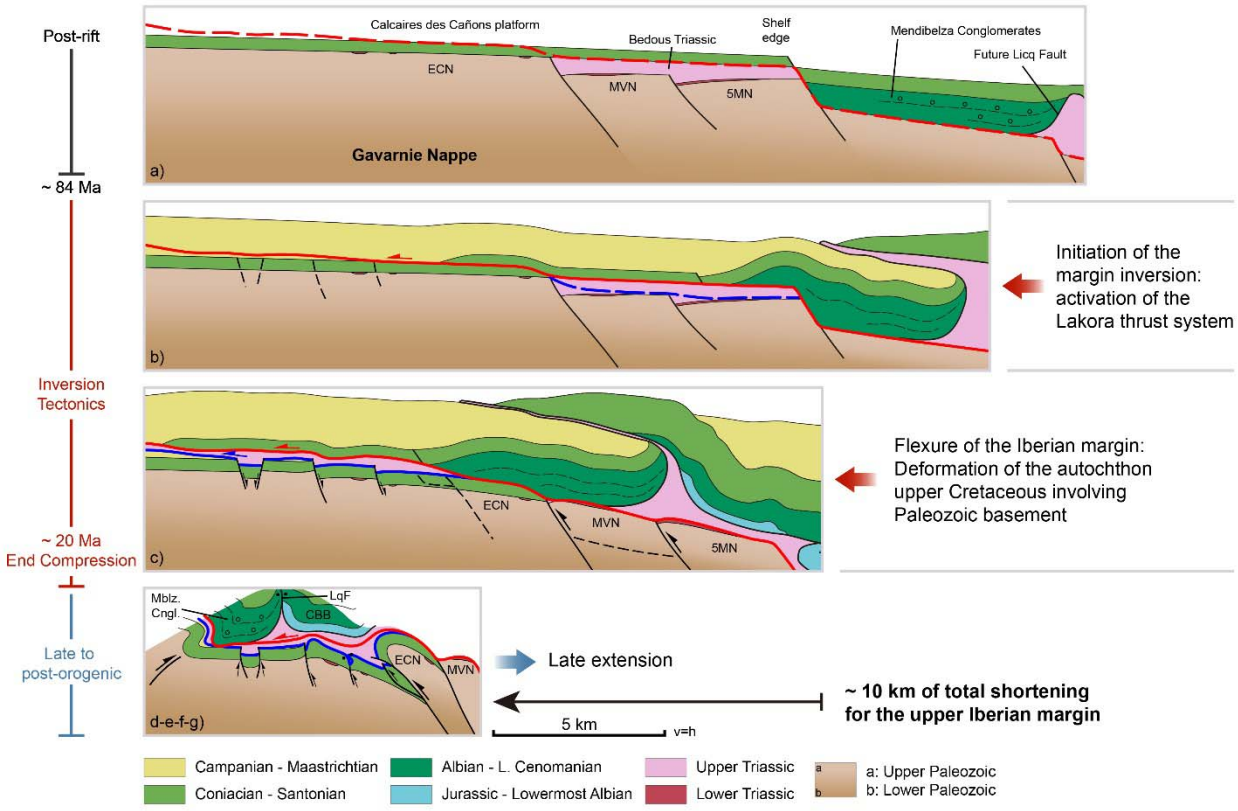

Fig. 13. Sketch illustrating the proposed sequence for the inversion of the uppermost Iberian margin in the eastern Eaux-Chaudes massif. It features the deformation of the footwall upper Cretaceous rocks in conjunction with the underlying Paleozoic metasediments and the overlying allochthonous Keuper sheet of the Bedous unit. Red line corresponds to the Lakora thrust

carrying the detached CBB and Mendibelza conglomerates. Blue line corresponds to the lower branch of the Lakora thrust carrying the allochthonous Keuper sheet on the ECU. Dashed lines show the location of future faults in the following steps. The structure of the pre-inversion stage (a) is modified from the model of hyper-extension of Teixell et al. (2016). The last stage (d-e-f) is based on the cross-section S4 from Fig. 8 for the ECN, MVN and 5MN. The kinematic evolution of the CBB is taken from Labaume & Teixell (2020). For explanation of acronyms, refer to the legend of the previous figure.

Supplementary Material

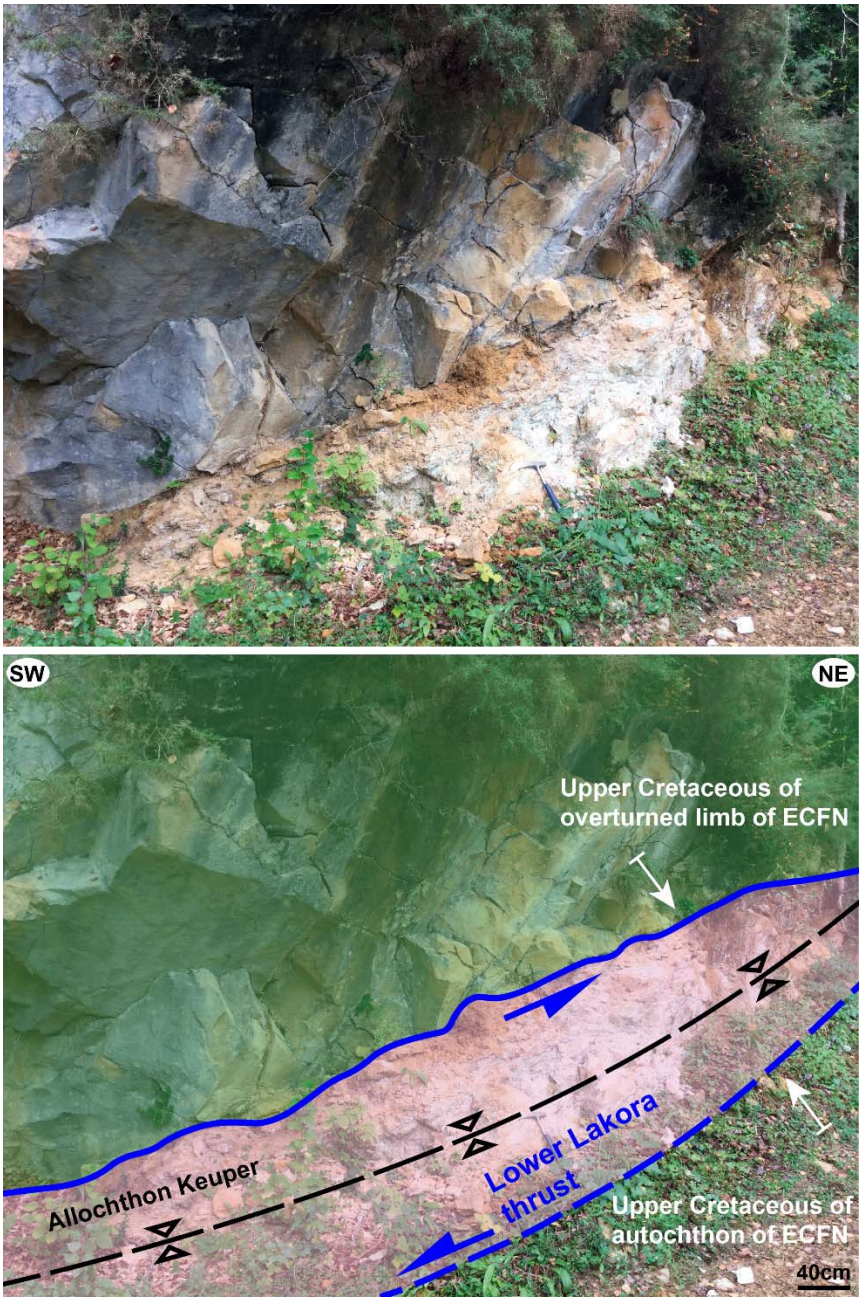

Sup. 1. Interpreted panorama of a pinched slice of hectometre-scale allochthon Keuper in the welded syncline conformed by the upper Cretaceous from the overturned limb and from the autochthon of the ECFN. The contact between the Keuper and autochthon upper Cretaceous is interpreted. The emplacement of the Keuper is performed by the Lower Lakora thrust at early stages of the Alpine compression.

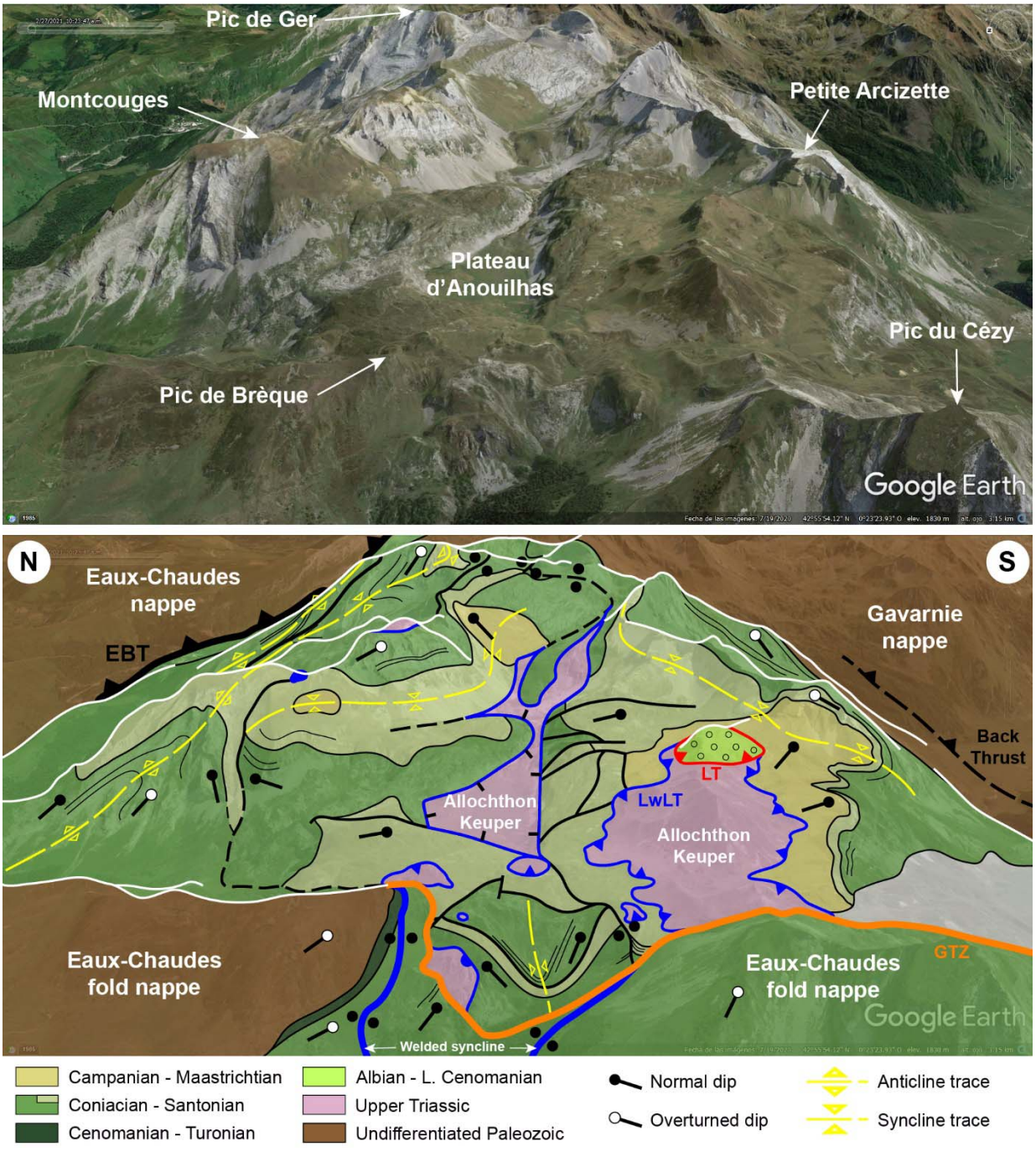

Sup. 2. Interpreted panorama of the transition from the western to the eastern sector of the ECM. At the bottom of the image the Eaux-Chaudes fold nappe is represented by the overturned polarity of the upper Cretaceous and the Paleozoic rocks. The transition to the east is defined by the orange line which conforms the Gourzy Transfer Zone. The eastern sector is characterized by fold structures with E-W-trend fold axis identified by yellow dashed lines. The

presence of the allochthon upper Triassic (Keuper facies) is substantially more representative and emplaced by the Lower Lakora thrust. A small outcrop of Mendibelza conglomerates, Albian in age, remain partially on the Keuper and on the Campanian flysch, carried by the Lakora thrust *s.l.* The Eaux-Bonnes thrust outcrops at the upper left edge of the image carrying the Paleozoic basement on top of the deformed autochthon upper Cretaceous. At the right border of the image the back thrust structure coetaneous to the emplacement of the Gavarnie nappe at the full-compression stage is interpreted. EBT: Eaux-Bonnes thrust; LT: Lakora thrust; LwLT: Lower Lakora thrust; GTZ: Gourzy Transfer Zone.

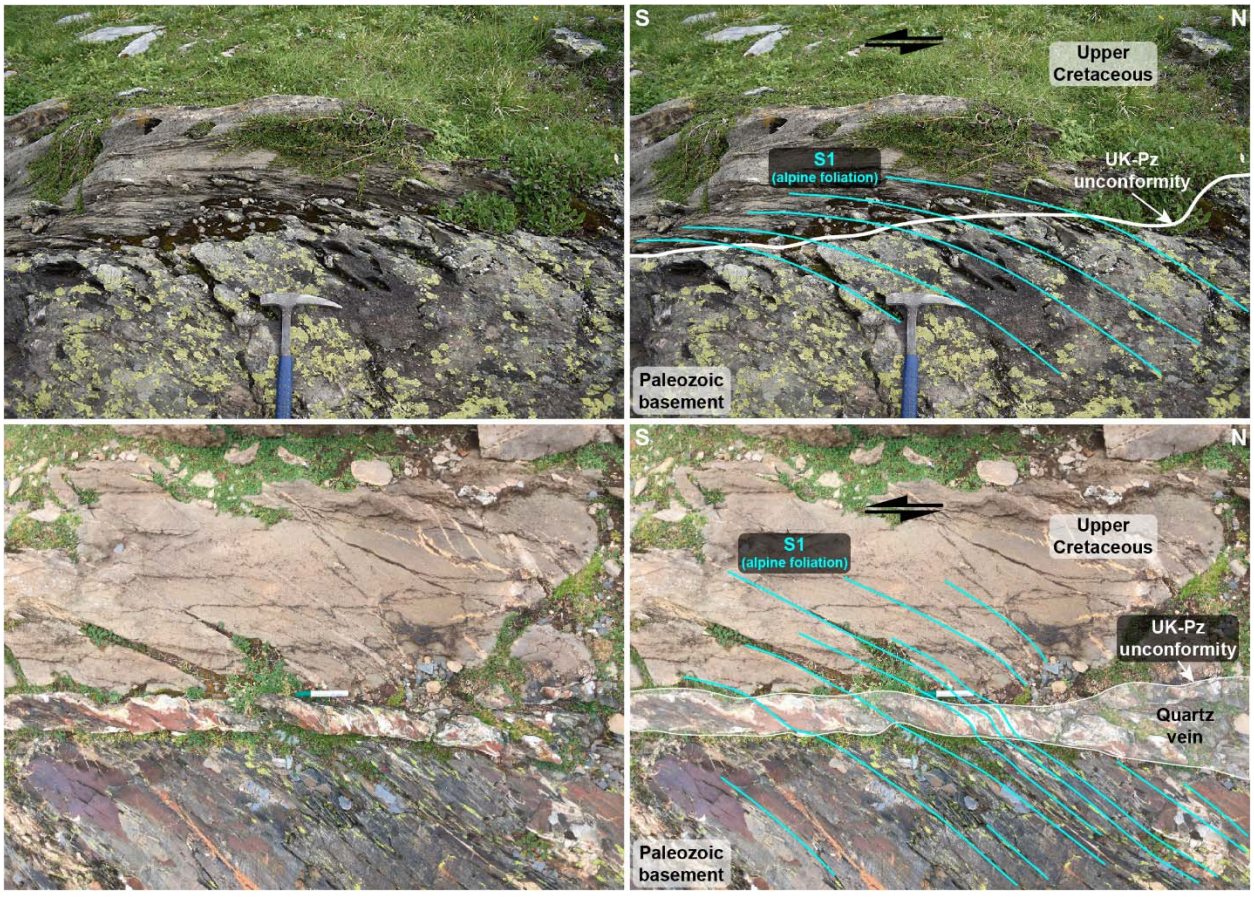

Sup. 3. Interpreted outcrops of the main unconformity between the Paleozoic basement and the upper Cretaceous where it is possible to recognize the refraction of the Alpine foliation along the

transition. This effect is enhanced in the areas where the unconformity is defined by a quartz vein.